Engineering of ion permeable planar membranes and polymersomes based on β-cyclodextrin-cored star copolymers

Haiqin Du, Sandra Kalem, Cécile Huin, Nicolas Illy, Guillaume Tresset, Fernando Carlos Giacomelli, Philippe Guégan

Journal Pre-proofs

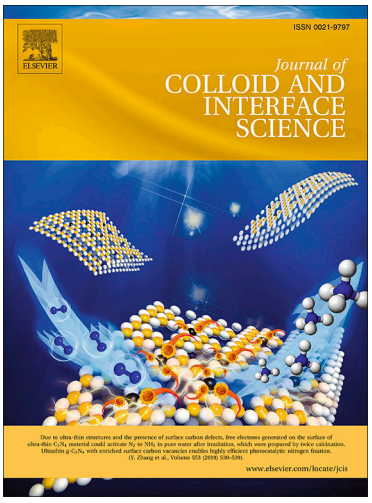

Engineering of Ion Permeable Planar Membranes and Polymersomes based on β-Cyclodextrin-Cored Star Copolymers

Haiqin DU, Sandra KALEM, Cécile HUIN, Nicolas ILLY, Guillaume TRESSET, Fernando Carlos GIACOMELLI, Philippe GUÉGAN

PII: S0021-9797(22)01738-6
DOI: https://doi.org/10.1016/j.jcis.2022.09.147
Reference: YJCIS 31088

To appear in: *Journal of Colloid and Interface Science*

Received Date: 19 July 2022
Revised Date: 9 September 2022
Accepted Date: 29 September 2022

Please cite this article as: H. DU, S. KALEM, C. HUIN, N. ILLY, G. TRESSET, F. Carlos GIACOMELLI, P. GUÉGAN, Engineering of Ion Permeable Planar Membranes and Polymersomes based on β-Cyclodextrin-Cored Star Copolymers, *Journal of Colloid and Interface Science* (2022), doi: https://doi.org/10.1016/j.jcis.2022.09.147

Engineering of Ion Permeable Planar Membranes and Polymersomes based on β-Cyclodextrin-Cored Star Copolymers

Haiqin DU[1], Sandra KALEM[1], Cécile HUIN[1,2], Nicolas ILLY[1], Guillaume TRESSET[3], Fernando Carlos GIACOMELLI[1,4], Philippe GUÉGAN[1]*

[1]Equipe Chimie des Polymères, Institut Parisien de Chimie Moléculaire (UMR-CNRS 8232), Sorbonne Université, 75252 Paris, France;

[2]Université d'Evry Val d'Essonne, Université Paris-Saclay, 91000 Evry, France

[3]Université Paris-Saclay, CNRS, Laboratoire de Physique des Solides, 91405 Orsay, France

[4]Centro de Ciências Naturais e Humanas, Universidade Federal do ABC, 09210-580 Santo André, Brazil

Highlights

1. Symmetric 14-armed βCD-cored star amphiphilic block copolymers βCD-(PBO-PGL)$_{14}$ were obtained with tunable arm block lengths, high purity and low polydispersity;

2. Star copolymers βCD-(PBO-PGL)$_{14}$ have similar self-assembly behavior compared to linear analogues (PGL-PBO-PGL);

3. Polymersomes made from βCD-(PBO-PGL)$_{14}$ have different ion permeability behavior compared to linear analogues (PGL-PBO-PGL);

Abstract

For polymersome-based nanoreactor purposes, we herein present the synthesis and characterization of well-defined star amphiphilic copolymers composed of a *beta*-cyclodextrin (βCD) core and seven poly(butylene oxide)-*block*-polyglycidol (PBO-PGL) arms per side (βCD-(PBO-PGL)$_{14}$). The self-assembly behavior of 14-armed βCD-(PBO-PGL)$_{14}$ and PGL-PBO-PGL (linear analogues without the βCD segment) was investigated using scattering techniques for comparison. The morphologies, including vesicles and micelles, are governed by the hydrophobic-to-hydrophilic (weight) ratio, regardless of the polymer architecture (linear or star). Interestingly, despite notable differences in polymer conformation, the produced supramolecular structures were evidenced to be fairly similar on the structural point of view. We subsequently investigated the ion permeability of the membranes of the self-assemblies focusing on the impact of the presence of βCD. The results demonstrated that the βCD-containing vesicular membranes are less permeable to H^+, compared with βCD-free vesicular membranes. The presence of βCD in planar membranes also influences the K^+Cl^- permeability to some extent. Thus, βCD-containing membranes can be considered as potential candidates in designing nano-containers towards applications where precise changes in environmental pH are required.

Keywords: self-assembly, polymersome, membrane permeability, amphiphilic copolymers, *beta*-cyclodextrin.

TOC :

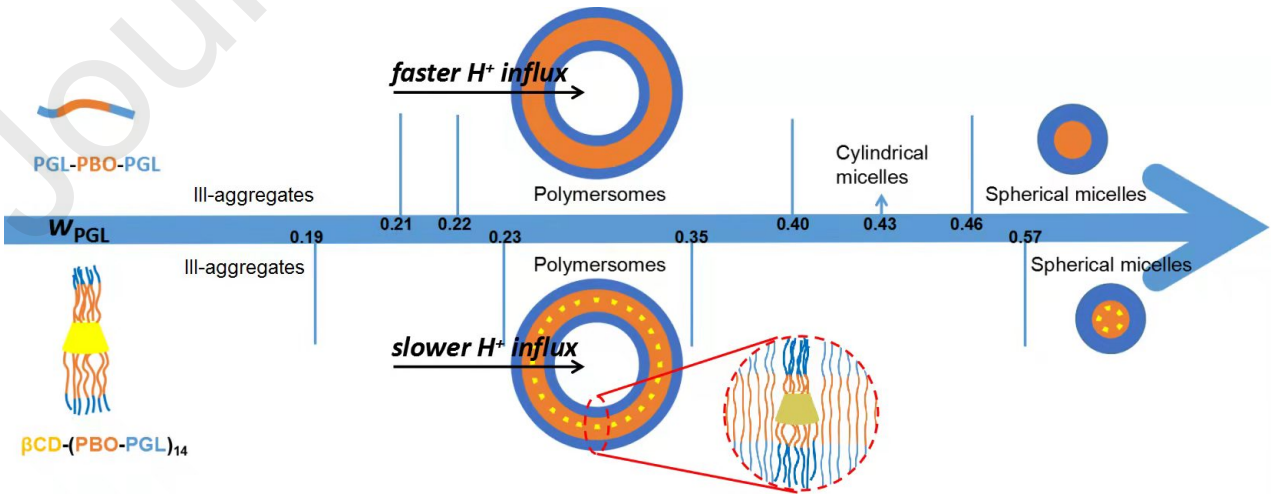

1. Introduction

Polymersomes are vesicles where the aqueous inner compartment is surrounded by a polymeric membrane *via* the self-assembly of amphiphilic polymers, including block and grafted copolymer [1−3]. Practical advantages of polymersomes over liposomes (vesicles obtained from the self-assembly of lipids) lie in their higher stability, chemical versatility and tunability of membrane thickness [2,4]. Compared to other self-assemblies such as micelles, polymersomes can be loaded with both hydrophilic and hydrophobic molecules, making them attractive for a variety of biotechnological applications [5−7]. Indeed, the vesicular structure of polymersomes has led to outstanding developments in cell-mimicking and nanocatalysis thanks to the compartmentalization feature [8]. Entrapping catalysts such as enzyme in a polymersome offers protection to the biological material from external harmful environments. The compartmentalization also makes enzymatic reactions more effective, taking advantage of the confinement effect [9]. Therefore, amongst a variety of other applications, enzyme-loaded polymersomes are promising tools to study the reactions occurring in organism [10] and to substitute dysfunctional organelles when they are further functionalized [11].

In this framework, membrane permeability is crucial to make the assemblies functional. High-molar-mass constituents of polymersomes generally produce robust and stable compartments, and consequently increase the barrier against substrate diffusion [12−14]. To date, only a few polymersomes were found to be intrinsically permeable to serve as versatile platforms towards the design of nanoreactors [15,16]. Accordingly, various strategies have been proposed to tune such property. The permeability of polymersomes has been regulated by making them responsive to external stimuli [6], or by modifications *via* post-polymerization methods [17], for instance. Compared with the methods where tedious treatments are commonly required, the use of a bio-inspired strategy, by inserting membrane proteins, was suggested as a more versatile way to regulate the permeability of polymeric vesicles [18].

Synthetic nanochannels possessing good structural stability have been also suggested as an alternative to the expensive and fragile bio-originated membrane proteins that can be inserted into lipid bilayers [19]. Amphiphilic *beta*-cyclodextrin (βCD)-based nanochannels is one of the earliest approaches in this regard [20]. βCD has a rigid truncated cone structure with a hydrophobic cavity and 21 hydroxyl groups thus permitting functional modifications [21]. In previous investigations, βCD-based amphiphilic derivatives and star βCD-containing polymers have been developed to form artificial nanochannels inserted into planar lipid bilayers, thus permitting the diffusion of ions and the translocation of ssDNA chains [22−25]. Ravoo's research

group for instance has developed a series of porous CD-based bilayered vesicles using amphiphilic cyclodextrin derivatives. α- or β-cyclodextrin was modified by aliphatic chains having 12 to 16 carbon atoms on its primary face and hydroxyethyl groups on the secondary face. The secondary face of the CD was then in contact with the aqueous media, while the aliphatic chains were oriented inward to form the bilayer. The thickness of the CD-based vesicles varied from 41.9 to 45.7 Å and the membranes varied from a fluid to a densely-packed state as the number of carbons on the aliphatic chains increased. The permeability of these vesicles was controlled by their thickness and melting temperature, while the cyclodextrins located at the surface of the vesicles provided a size-selective distinction [26,27]. Thin-film composites embedding cyclodextrin were also developed for nanofiltration membranes, and the cyclodextrins provided an increased permeability and selectivity to the materials [28,29].

Nevertheless, to the best of our knowledge, embedding cyclodextrins in a polymer membrane to modulate its permeability and selectivity has never been attempted, neither for 3D vesicular nor for 2D planar membranes. Hence, the present work aimed to design polymeric membranes having cyclodextrins embedded in the hydrophobic segment *via* the self-assembly of amphiphilic βCD-cored star copolymers. The influence of βCD on the ion permeability and selectivity was investigated and systematically compared to assemblies produced using linear analogues. The membrane permeability to proton (H^+), potassium (K^+) and chloride (Cl^-) has been evaluated because they are involved in the maintenance of cell homeostasis [30,31].

Accordingly, βCD-based star amphiphilic copolymers βCD-$(PBO\text{-}PGL)_{14}$, composed of a βCD core and seven poly(butylene oxide)-*block*-polyglycidol arms on each side of the βCD (primary and secondary rim), have been firstly synthesized and characterized. Then, the self-assembly behavior has been studied and ultimately, polymersome permeability to H^+ have been investigated *via* fluorescence spectrometry. In addition, planar membrane permeability to K^+Cl^- has been investigated using the black lipid membrane technique. We discuss the influence of the βCD cavity with regard to the permeability to these different ions.

2. Materials and Methods

2.1. Materials

The βCD-based initiator, per(2-O-methyl-3,6-di-O-(3-hydroxypropyl))-βCD (βCD-$(OH)_{14}$), was synthesized following a published procedure [25] (NMR spectra - Figure S1 of Supplementary Information). Ethoxyethyl glycidyl ether (EEGE) was prepared using a published method [32] (NMR spectra - Figure S2 of Supplementary Information). Other chemicals for polymerization are butylene oxide (BO, 99%,

Sigma−Aldrich), DMF (anhydrous, 99.8%, Sigma−Aldrich), toluene (anhydrous, collected from the MB SPS COMPACT solvent purification system equipped in glovebox) and *t*BuP$_4$ (0.8 M in n-hexane, Sigma−Aldrich). βCD-(OH)$_{14}$ was intensively dried following a published procedure [25] and freshly used. BO, EEGE and DMF were dried over CaH_2 (Sigma−Aldrich) twice and stored in glovebox before use. Toluene was used as received. *t*BuP$_4$ was stored in glovebox before use and used as received. All the chemicals were charged into reaction container in the glovebox (MBRAUN) which is equipped with a gas purification system (molecular sieves and copper catalyst) and dry over argon atmosphere to ensure the moisture content (H_2O) less than 0.5 ppm as monitored by an MB-MO-SE1 moisture probe.

The chemicals for common uses including $CHCl_3$ (VWR), decane (anhydrous, Sigma–Aldrich), diethyl ether (Et_2O, VWR), methanol (MeOH, VWR), HCl (37%, Sigma−Aldrich), NaOH (Sigma−Aldrich), NaCl (VWR), $NaHCO_3$ (VWR), Na_2HPO_4 (Sigma−Aldrich), KCl (Sigma−Aldrich), KH_2PO_4 (Sigma−Aldrich), $MgSO_4$ (VWR) and 8-hydroxypyrene-1,3,6-trisulfonic acid trisodium salt (HPTS, Sigma−Aldrich, 99%) were properly stored and used as received.

Linear amphiphilic triblock copolymers, polyglycidol-*block*-poly(butylene oxide)-*block*-polyglycidol (PGL-PBO-PGL), used for comparison purpose, were synthesized following the same procedure as previously reported [33]. The characteristics of the linear copolymers were listed in Table S1 of the Supplementary Information File.

2.2. Synthesis and characterization of star copolymers

2.2.1 Synthesis of star copolymers

The 14-armed βCD-cored star copolymers, βCD-(PBO$_m$-PGL$_n$)$_{14}$ with *m* and *n* being respectively the numbers of BO and GL units per arm, were synthesized following a published method [25] with adaptions. A typical procedure is described for the synthesis of βCD-(PBO$_{24}$-PGL$_6$)$_{14}$: BO (0.1124 g, 1.70 mmol, 113 eq) and *t*BuP$_4$ (0.8 M in *n*-hexane; 52.5 μL, 0.042 mmol, 2.8 eq) were sequentially added into the solution of βCD-(OH)$_{14}$ (30.66 mg, 0.015 mmol, 1 eq) in DMF (0.26 mL). The reaction mixture was stirred at 30 °C for 48 hours. Then, the solvent DMF and the unreacted monomer BO were removed *via* distillation on vacuum line. The residue was dissolved in toluene (1.2 mL) followed with the sequential additions of BO (0.3607 g, 5.00 mmol, 334 eq) and *t*BuP$_4$ (0.8 M in *n*-hexane; 26.25 μL, 0.021 mmol, 1.4 eq). The reaction mixture was stirred at 30 °C for 72 hours. Subsequently, EEGE (0.3052 g, 2.09 mmol, 139 eq) was charged into the reaction medium so that copolymerization was performed at 30 °C for 72 hours. Then, drops of DI H_2O were added into the reaction medium. The mixture was concentrated, and the residue was dissolved in Et_2O and washed with DI H_2O. The organic solution was dried by $MgSO_4$. After filtering out the solid, the filtrate was concentrated giving the

copolymerization product. The obtained copolymerization product, with a composition of BO/EEGE/βCD = 431/139/1 (Mn = 53.4 kg mol^{-1}; 732.7 mg, 0.014 mmol), was dissolved in MeOH (8.6 mL). Then, into this solution, a HCl solution (2 M in MeOH; 0.96 mL, 1.91 mmol) was added. The mixture was stirred at room temperature for 6 hours before adding $NaHCO_3$ (0.48 g, 5.7 mmol) into the mixture. The resulting solid was filtered out and the collected filtrate was concentrated to give the crude product, which was further purified by dialysis against MeOH with a regenerated cellulose membrane (MWCO 10 kDa, Spectrum Laboratories, Inc.). The final purified product was obtained after removing the solvent.

2.2.2 Characterization of the star copolymers

^{1}H NMR spectra were recorded on a Bruker Ultra Shield 300 NMR spectrometer routinely (300 K) and analyzed with MestReNova 9.1.0 software using the residual proton signals of the deuterated solvents as the internal reference.

Size-exclusion chromatography (SEC) characterizations were performed in DMF or THF. In DMF, the measurements were carried on a Viscotek gel permeation chromatography system (TDA 305) equipped with one PSS-GRAM 30 Å column (8 mm × 300 mm) and two PSS GRAM 1000 Å columns (8 mm × 300 mm) maintained at 60 °C. DMF (containing 1.0 g L^{-1} lithium bromide as an additive) was used as the mobile phase at a flow rate of 0.8 mL min^{-1}. All polymers were injected at a concentration of 5 mg mL^{-1} after filtration through a 0.2 μm syringe filter. In THF, the measurements were carried out on three PL Gel Mixte C 5 μm columns (7.5 × 300 mm) maintained at 40 °C, coupled with two modular detectors: a differential refractive index (RI) detector (Viscotek 3580) and a diode array UV detector (Shimadzu SPD20-AV). THF was used as the mobile phase at a flow rate of 1 mL min^{-1}. All polymers were injected at a concentration of 5 mg mL^{-1} after filtration through a 0.45 μm syringe filter. In both cases, the OmniSEC 5.12 software was used for data acquisition and analysis. The number-average molar mass (Mn$_{SEC}$), weight-average molar mass (Mw$_{SEC}$) and polydispersity index ($Đ$ = Mw$_{SEC}$/Mn$_{SEC}$) were determined with a calibration curve based on narrowly distributed poly(methyl methacrylate) (PMMA) standards (from Polymer Standard Services) using a RI detector.

2.3. Preparation and characterization of the self-assemblies

2.3.1 Preparation of the self-assemblies

The self-assemblies of star amphiphilic copolymers were obtained using the thin-film rehydration protocol. Typically, the polymer (5.0 mg) was firstly dissolved in MeOH (2.5 mL). Subsequently, MeOH was removed by rotavapor (40 °C, 5 mbar, 30 min) to get the polymer film on the inner wall of the sample vial. The polymer thin-film was

then rehydrated using DI H_2O (5.0 mL). After stirring for adequate time, the film sufficiently detached from the inner wall giving a suspension. The suspension was extruded through a 0.45 μm PTFE syringe filter repeatedly (5 times, in one direction).

2.3.2 Characterizations of the self-assemblies

Dynamic light scattering (DLS) characterization was performed using a Zetasizer Nano ZS90 at 20 °C. The averaged intensity autocorrelation functions were evaluated using non-negative least-squares (NNLS) analysis implemented in the Zetasizer software to produce the intensity particle size distribution (PSD) curves. The hydrodynamic radius (R_H) and polydispersity index (PDI) of particles were reported as the Z-average radius and corresponding PDI value given by the Zetasizer software (Cumulant analysis) based on 5 measurements. The straightforward Stokes-Einstein equation was used to compute the R_H values.

Static light scattering (SLS) measurements were conducted on a Zetasizer Nano ZS90 at 20 °C by measuring the light scattering monitored at a scattering angle ($\theta = 90°$) as a function of the polymer concentration. The molecular weight of self-assembled nanoparticle ($M\mathrm{w}_{\mathrm{NPs}}$) was estimated using the Debye plot. The aggregation number (Nagg) was further calculated using the Equation 1.

$$N\mathrm{agg} = \frac{M\mathrm{w}_{\mathrm{NPs}}}{M\mathrm{w}_{\mathrm{polymer}}} \quad (1)$$

where $M\mathrm{w}_{\mathrm{polymer}}$ is the molar mass of the copolymer.

Small-angle X-ray scattering (SAXS) measurements were performed with the SWING beamline at SOLEIL synchrotron facility (Saint-Aubin, France). The wavelength was set to 1 Å and the sample-to-detector distance was 2 m, which provided scattering wavenumbers ranging from 0.004 to 0.5 $Å^{-1}$. The samples were automatically injected into a through-flow capillary. For each sample, about 30 two-dimensional scattering images were recorded on an Eiger 4 M Dectris detector with an exposure time of 1 s while pushing the sample to avoid radiation damage. The scattering intensities were converted into absolute units after subtracting the contribution of the solvent using the FOXTROT software package. The produced SAXS patterns were further analyzed using the SASfit software (Paul Scherrer Institute, Switzerland).

2.4. Permeability of polymersome membranes to H^+

2.4.1. Preparation of HPTS-loaded polymersomes (HPTS-pos)

The HPTS-loaded polymersomes (named HPTS-pos) were also prepared by thin-film rehydration [34,35]. The polymer (10.0 mg) was dissolved in MeOH (4 mL). Then, MeOH was removed by rotavapor (5 mbar, 40 °C, 30 min) to get the thin polymer

film sited on the inner wall of a glass vial. The film was subsequently rehydrated with HPTS solution (10.0 mL, 0.2 mg mL^{-1} in phosphate-buffered saline solution - PBS). The mixture was stirred at room temperature allowing the film to detach from the inner wall and to be suspended homogeneously. The rehydrated suspension was extruded through a 0.45 μm PTFE syringe filter repeatedly (10 times, in one direction) to remove dust and get a homogeneous suspension [36]. Afterwards, the extruded suspension was dialyzed against PBS with a regenerated cellulose membrane (MWCO 3.5 kDa, Spectrum Laboratories, Inc.). The dialysis reservoir (1 L, PBS) was changed as many times as needed to totally remove the unencapsulated HPTS probes. Lastly, the dialysis retention solution, namely the suspension solution of HPTS-pos, was collected and freshly used.

2.4.2. Permeability of polymersome membranes to H^+

The investigation was conducted following a published protocol [34] with minor modifications. The HPTS-pos suspension (2.5 mL) was charged into a quartz cell (1 cm^2 × 4 cm). Then, fluorescence excitation spectrum of the solution was continuously recorded for 10 minutes at a time interval of 0.5 minutes. Subsequently, a drop of HCl solution (1 M, 10 μL) was added into the suspension. The excitation spectrum of the mixture was immediately recorded with the system being in a steady state (without stirring). The continuous recording was performed for 90 minutes at an interval of 0.5 minutes. All the spectra were recorded on a Cary Eclipse fluorophotometer at room temperature, the emission wavelength being 509 nm and the ex-slit and em-slit both 2.5 nm. The obtained spectra were analyzed using the OriginPro 8 software to extract a plot of intensity ratio (I_{455}/I_{402}) versus time, in which I_{455} and I_{402} were the excitation intensities at 455 nm and 402 nm, respectively. The intensity ratio plot was further interpreted into a plot of the interior pH of polymersomes (pH_f) as a function of time, with the aid of a pH calibration curve, which was constructed under the same characterization conditions (Supplementary Information). As a control, the HPTS solution, having the same HPTS concentration as the one of HPTS-pos suspension, was used and studied with the same protocol.

2.5. Permeability of planar polymeric membranes to K^+Cl^-

The measurements were performed at room temperature on a black lipid membrane set-up which was equipped with an amplifier (BLM Axopatch 200B-1). Firstly, planar membrane was painted on a 150-μm window of the PTFE separator of BLM base according to a published method [37]. Typically, polymer (5.0 mg) was dissolved in a mixture of $CHCl_3$ (200 μL), decane (200 μL) and MeOH (100 μL) (polymer concentration of 10 mg mL^{-1}). One-μL of the solution was deposited/painted on the surface of the 150-μm window and left for 1 hour at room temperature. The painting operation was repeated once more, and air-dried for one hour to form a "pre-layer" on

the window. Subsequently, the pre-treated window was settled in the BLM base and the two chambers were filled with concentrated KCl solution (1 M). Lastly, a tiny amount of the polymer solution was introduced with a pipette, adjacent to the separator, to form the planar polymeric membrane covering the window. Then, current intensity was recorded as a function of time when a constant voltage was applied at both sides of the membrane, with Ag/AgCl electrodes inserted in each of the chambers. Signals were acquired at 100 kHz and filtered at 10 kHz. The amplifier was connected to a digitizer (Measured Computing Digitizer), and both were connected to a computer where the Labview software allows visualizing the results. All the data were analyzed using IGOR software.

3. Results and Discussion

3.1. Synthesis and structural characterization of star copolymers

The βCD derivative, per(2-O-methyl-3,6-di-O-(3-hydroxypropyl))-βCD (βCD-$(OH)_{14}$), has been proven to possess 14 hydroxyl functions of equal initiation reactivity in anionic ring-opening polymerizations [23,38,39]. Thus, the βCD-$(OH)_{14}$ initiator was used to synthesize the βCD-cored star copolymers bearing 14 poly(butylene oxide)-*block*-polyglycidol arms denoted as βCD-$(PBO_m\text{-}PGL_n)_{14}$ with *m* and *n* being respectively the numbers of BO and GL units per arm.

The synthetic procedure was adapted from published procedures [25,40,41] and illustrated in Scheme 1.

Scheme 1. Synthetic route used in the preparation of βCD-$(PBO_m\text{-}PGL_n)_{14}$ star copolymers.

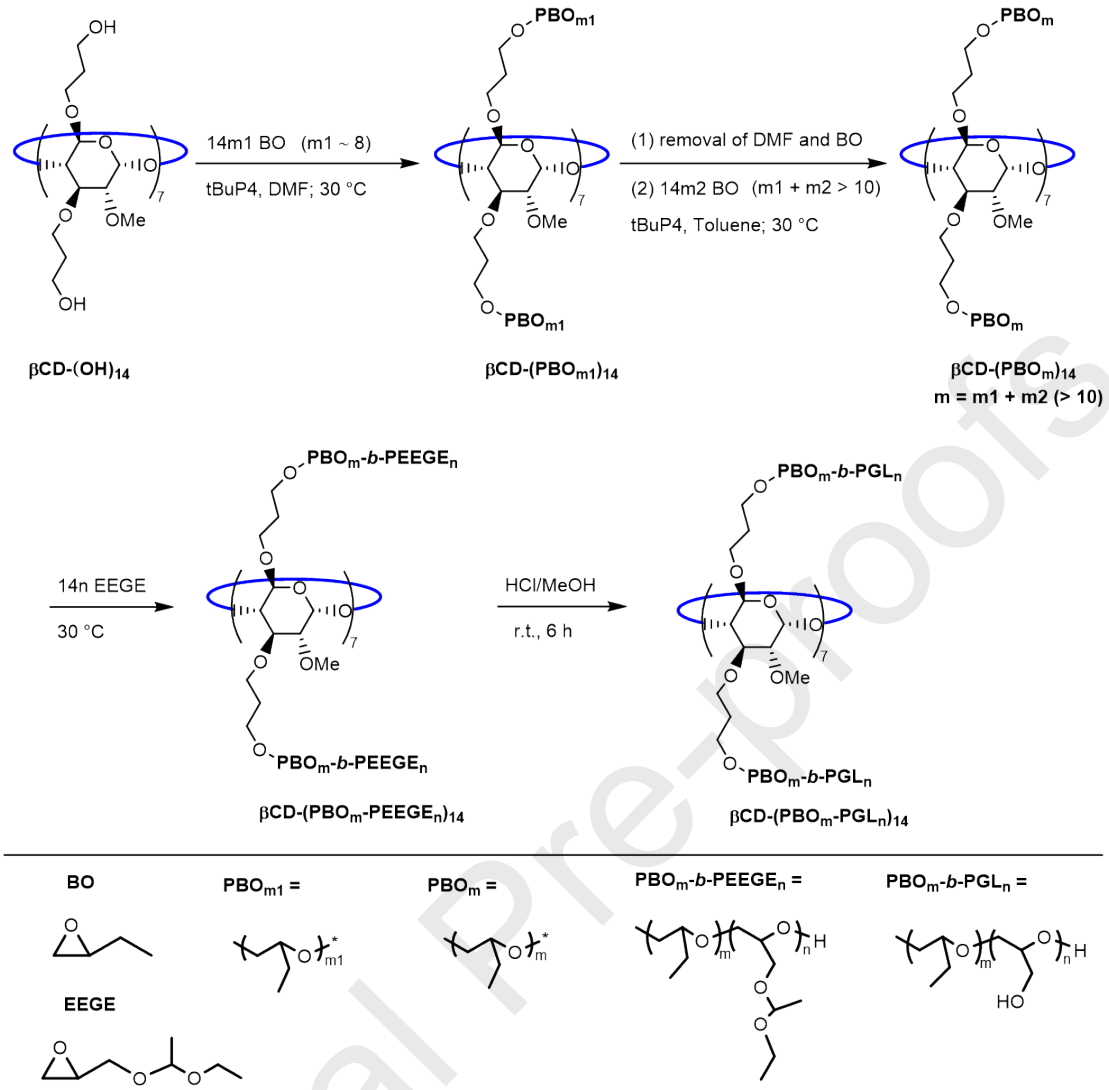

This procedure includes a two-step homopolymerization of BO, a subsequent block copolymerization of EEGE and a final deprotection to reveal GL units. It is worth mentioning that the stepwise homopolymerization of BO is optional depending on the targeted length of PBO blocks. Indeed, when short PBO blocks (m < 10) are targeted, the first homopolymerization step is merely performed in DMF, whereas when long PBO blocks (m ≥ 10) are targeted, two homopolymerization steps are required and performed respectively in DMF then in toluene, as pointed out in the synthetic procedure (Scheme 1). The stepwise homopolymerization strategy was proposed to overcome the limitation of PBO length obtained in DMF, a solvent necessarily required to dissolve the initiator [39]. The details and results are given in the Supplementary Information File (Table S2).

Concerning the synthesis of βCD-(PBO_{24}-PGL_6)$_{14}$, the first homopolymerization of BO was performed in DMF with the feeding ratio of $[BO]_1/[tBuP_4]_1/[\beta CD]_0$ = 113/2.8/1. After 48 hours, BO conversion was calculated from the ^{1}H NMR spectrum,

as p_{BO1} = 0.86, based on the integrals of the epoxide proton and the methyl protons (Figure S4A, SI). It is important to note that the anomeric proton of the glucopyranose unit is hardly detected and cannot be accurately integrated, preventing the *M*n determination by ^{1}H NMR.

The second homopolymerization was then performed in toluene with the molar ratio of $[BO]_2/[t\text{BuP}_4]_2/[\beta CD]_0$ = 334/1.4/1, for 72 hours. At the end, nearly all BO monomer was consumed (p_{BO2} = 0.99) as checked by ^{1}H NMR (Figure S4B, SI). It can be seen that the anomeric proton is undetectable, considering the high degree of polymerization (*X*n) of PBO.

Subsequently, the copolymerization was conducted with the ratio of $[EEGE]/[\beta CD]_0$ = 139/1, for 48 hours. At the end, EEGE was totally consumed (p_{EEGE} = 1), as also confirmed by ^{1}H NMR (Figure S4C, SI), where the peaks attributed to the protons of PEEGE are only detected. At this point, the synthesis of PBO and PEEGE blocks is witnessed.

After quenching and removing $t\text{BuP}_4$, the copolymerization product PBO-PEEGE was obtained (Figure S5A, SI). At last, the acetal groups of EEGE units were cleaved, giving the crude deprotection product (Figure S5B, SI), evidenced by the disappearance of the characteristic peaks of EEGE units.

The intermediate and the final crude products were also characterized by SEC, as displayed in Figure 1A. The product obtained at the end of the first homopolymerization of BO is firstly analyzed. The narrowly distributed peak, centered at 23.7 mL, refers to the star PBO with a molar mass around 8 kg mol^{-1} determined using the PMMA standard (Table S3, SI). No specific peak could be attributed to free cyclodextrin initiator (*M*n = 2044 g mol^{-1}). However, a bump is hardly detected around 26.0−27.0 mL, attributed to the by-product resulting from the initiation by residual water entrapped in the βCD cavity [23,39], a linear PBO, denoted as HO-PBO-OH.

Trace b portrays the product obtained at the end of the second homopolymerization of BO. The peak centered at 21.9 mL refers to star PBO, while a small peak around 24.1 mL is attributed to linear by-product. Both peaks shift towards the lower elution volume part, compared with those in trace a, witnessing molar mass increases.

Trace c is the copolymerization product, resulting from the addition of PEEGE blocks, showing a further shift to 21.5 mL of the peak attributed to star PBO-PEEGE and a shift to 23.5 mL of the peak assigned to the linear by-product. The by-product consisted of linear PEEGE-PBO-PEEGE, deriving from HO-PBO-OH. Transfer-to-monomer and back-biting reactions in the ring-opening polymerization of EEGE have already been reported [44,45]. However, the characteristic peaks of allylic

end groups around 6.6 ppm are not detected in the ^{1}H NMR spectrum (Figure S4C, SI), witnessing for the very low occurrence of such reactions.

Trace d displays the crude deprotection product, which was obtained by removing the acetal groups from PEEGE of both star copolymer and linear by-product in acidic conditions. Compared with the peaks in trace c, the two peaks here both shift to larger elution-volume side, to 21.7 mL and 23.7 mL respectively for the star PBO-PGL and the linear by-product, in accordance with the loss of protecting groups.

The crude deprotection product was further purified, and the result is demonstrated in Figure 1B. It clearly shows that the linear impurities, mainly issued from water initiation as aforementioned, were almost removed without changing the molar mass of the star polymer.

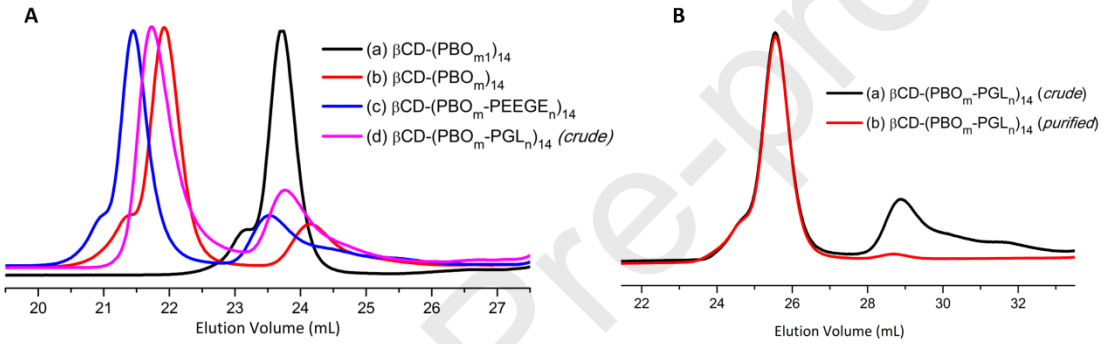

Figure 1. SEC traces of the intermediate and final products for the synthesis of βCD-(PBO$_{24}$-PGL$_6$)$_{14}$: (A) SEC-THF traces of the reaction media obtained at the end of (a) the first and (b) the second homopolymerization of BO, and traces of (c) copolymerization product (without *t*BuP$_4$), and (d) crude deprotection product. Characterizations were performed in THF at 40 °C using a RI detector. (B) SEC-DMF traces of (a) crude and (b) purified deprotection product. Characterizations were performed in DMF at 60 °C using a RI detector.

To estimate the purity of the intermediate and final products, namely the fraction of star polymer in each product (*f*), SEC peak areas (recorded with a RI detector) were used in the following equation:

$$f = \frac{A_s}{A_s + A_l} \quad (2)$$

where A_s and A_l are respectively the peak areas of star polymer and linear by-product, reported by the OmniSEC 5.12 software.

Accordingly, based on product purity (*f*), monomer feeding ratios

($[BO]_1/[BO]_2/[EEGE]/[\beta CD]_0$) and monomer conversions (p_{BO1}, p_{BO2} and p_{EEGE}), the theoretical formulae of the star polymers, including βCD-$(PBO_{m1})_{14}$, βCD-$(PBO_m)_{14}$, βCD-$(PBO_m\text{-}PEEGE_n)_{14}$ and βCD-$(PBO_m\text{-}PGL_n)_{14}$ were estimated (Table S3, SI). The characterization results indicate that the final product, βCD-$(PBO_{24}\text{-}PGL_6)_{14}$, has the desired length of PBO blocks with a low dispersity ($Đ$ = 1.05) and a satisfactory purity (f = 0.98).

The same procedure was applied to prepare a set of star amphiphilic copolymers with systematic variations in the length of PBO block and the weight fraction of PGL block (w_{PGL}). The copolymers were characterized by ^{1}H NMR and SEC (Figure S10), and the results are listed in Table 1 according to the w_{PGL}. It can be seen that each star polymer had a high purity (f) and a low dispersity ($Đ$), proving that the synthetic procedure is reproducible.

Table 1. Characteristics of βCD-$(PBO_m\text{-}PGL_n)_{14}$ according to the weight fraction of PGL blocks (w_{PGL}).

Entry	$[BO_0/[EEGE]_0/[\beta CD]_0$[a]	p_{BO}[b]	p_{EEGE}[b]	f[c]	Formula[d]	w_{PGL}[d]	$Mn_{theo.}$[d] (kg mol^{-1})	Mn_{SEC}[e] (kg mol^{-1})	$Đ$[e]
1	640/186/1	0.98	1	0.97	βCD-$(PBO_{30}\text{-}PGL_4)_{14}$	0.11	35.8	35.3[e']	1.08[e']
2	431/140/1	0.99	1	0.98	βCD-$(PBO_{24}\text{-}PGL_6)_{14}$	0.19	32.7	36.1	1.05
3	339/209/1	0.99	1	1	βCD-$(PBO_{22}\text{-}PGL_7)_{14}$	0.23	31.2	26.1	1.03
4	252/158/1	0.99	1	0.99	βCD-$(PBO_{13}\text{-}PGL_6)_{14}$	0.28	21.4	24.9	1.11
5	112/78/1	0.94	0.98	0.99	βCD-$(PBO_7\text{-}PGL_5)_{14}$	0.35	13.9	16.3	1.07
6	158/206/1	1	1	0.97	βCD-$(PBO_8\text{-}PGL_{12})_{14}$	0.57	22.2	28.1	1.05
7	91/211/1	0.98	0.89	0.94	βCD-$(PBO_6\text{-}PGL_{14})_{14}$	0.62	22.2	25.6	1.07

[a]The feeding ratio of BO was the total ratio taking into account both homopolymerizations when two homopolymerizations were performed; [b]The conversions of BO (p_{BO}) and EEGE (p_{EEGE}) were determined by ^{1}H NMR. BO conversion (p_{BO}) was the conversion at the end of the second homopolymerization when two homopolymerizations were performed; [c]The fraction of star copolymer in product, *i.e.*, the product purity (f) was estimated from SEC peak areas using Equation 2; [d]Theoretical formula of star copolymer was calculated based on monomer feeding ratios, monomer conversions (p) and the fraction of star copolymer (f). The weight fraction of

PGL blocks (w_{PGL}) was defined as the molar mass ratio of PGL blocks to star copolymer. Theoretical molar mass (Mn$_{theo.}$) was derived from theoretical formula; [e,e'] SEC characterizations were performed [e] in DMF at 60 °C or [e'] in THF at 40 °C, and the results were determined with PMMA as the standard and using a RI detector.

3.2. Self-assembly of star copolymers

The self-assemblies were obtained by the thin-film rehydration method [36,46], with a final concentration of 1 mg mL^{-1} in DI water. The thin film of βCD-(PBO$_m$-PGL$_n$)$_{14}$ deposited on the inner wall of a glass vial was rehydrated by DI water, producing suspensions of self-assemblies.

Firstly, according to the visual appearance and the recorded DLS signals of the rehydrated suspensions before and after filtration, the set of star copolymers was classified into three groups. The first group embraces βCD-(PBO$_{30}$-PGL$_4$)$_{14}$ and βCD-(PBO$_{24}$-PGL$_6$)$_{14}$. Both suspensions were turbid and heterogeneous with many visible aggregates, which have irregular size and shape (by eye) and tended to precipitate. Both turbid suspensions turned clear (colorless and transparent) and undetectable by DLS (Figure S11A) after being extruded once through a 0.45 μm syringe filter. In such cases, the small length of PGL blocks and the very high content of PBO presumably limit the colloidal stability of the self-assemblies in water since van der Waals interactions are supposed to be dominating. The second group contains βCD-(PBO$_{22}$-PGL$_7$)$_{14}$, βCD-(PBO$_{13}$-PGL$_6$)$_{14}$ and βCD-(PBO$_7$-PGL$_5$)$_{14}$: the obtained suspensions were white-bluish and homogeneous, without aggregates visible by naked eyes. The suspensions were also evidenced to be stable as a function of time. The samples remained white-bluish and homogeneous after 5 extrusions through a 0.45 μm filter, and the particle size became more narrowly distributed after the extrusions (Figure S11B) benefitting from the thin film rehydration method [35,36]. The third group concerns βCD-(PBO$_8$-PGL$_{12}$)$_{14}$ and βCD-(PBO$_6$-PGL$_{14}$)$_{14}$: the prepared samples were colorless and transparent and both were stable, resulting from the large length of PGL blocks. The suspensions changed little after extrusions because the small sizes (Figure S11C).

The suspensions of the second and third groups were characterized by DLS and SLS to get information on the size and molecular weight of the self-assembled particles. Figure 2A displays the representative DLS characterization for self-assemblies produced from βCD-(PBO$_{13}$-PGL$_6$)$_{14}$ and βCD-(PBO$_6$-PGL$_{14}$)$_{14}$. These two star polymers are close in molar mass but significantly different in hydrophobic-to-hydrophilic ratio: w_{PGL} is 0.28 for βCD-(PBO$_{13}$-PGL$_6$)$_{14}$ and 0.62 for βCD-(PBO$_6$-PGL$_{14}$)$_{14}$. It can be seen that the self-assembled particles present

monomodal intensity particle size distribution curves with average R_H of 90 nm and 6 nm (Table 2). Along with the *N*agg values, respectively 1400 and 8 (Table 2), it is suggested that the self-assemblies of βCD-$(PBO_{13}$-$PGL_6)_{14}$ and βCD-$(PBO_6$-$PGL_{14})_{14}$ are respectively vesicles and micelles. To ascertain this analysis, the self-assemblies were further characterized by SAXS. Figure 2B displays the SAXS patterns which respectively fit well into a bilayered vesicle and a core-shell form factor, undoubtedly and robustly confirming the presence of different morphologies as suggested by the light scattering analyses.

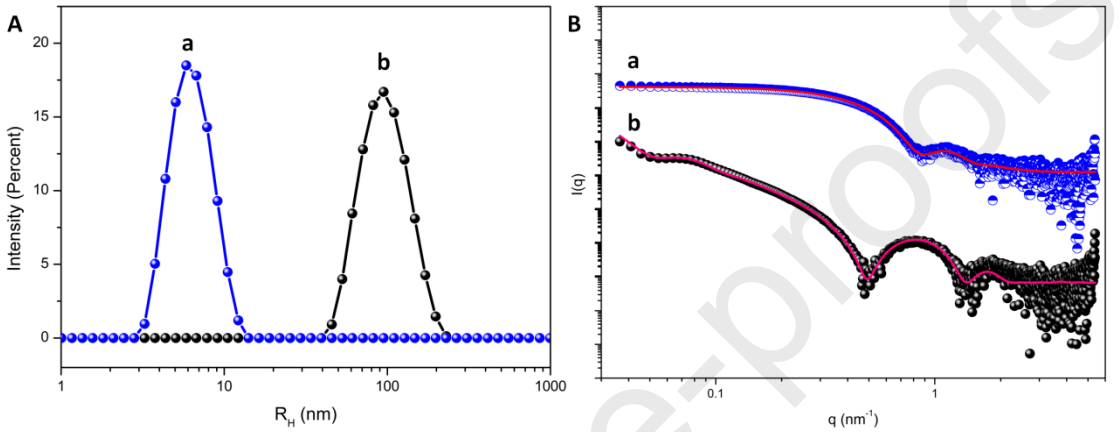

Figure 2. (A) Intensity particle size distribution curves, and (B) SAXS profiles (dots) with respective curve fittings (solid lines) of the self-assemblies of (a) βCD-$(PBO_6$-$PGL_{14})_{14}$ and (b) βCD-$(PBO_{13}$-$PGL_6)_{14}$. SAXS profiles were fitted by using a core-shell (a) and a bilayered vesicle (b) form factor.

The vesicular morphology is suggested for βCD-$(PBO_{13}$-$PGL_6)_{14}$ (trace b in Figure 2B) by the good fitting into the bilayered vesicle form factor. The presence of the typical q^{-2} power law dependence of the intensity at the lower *q*-range supports this conclusion. The upward profile extends beyond the lowest *q*-region accessed (q = 0.04 nm^{-1}) indicating that even in such length scale ($q = 2\pi/0.04$ $nm^{-1} \sim 157$ nm) the structures are present in agreement with the DLS data ($D_H = 2R_H = 180$ nm). The characteristic oscillation located at $q \sim 0.5$-1.5 nm^{-1} is therefore associated to the vesicle membrane thickness. The fitting using the bilayered vesicle form factor implemented in the SASfit software included as adjustable parameters the radius of the inner compartment consisting of water (R_c), the thickness of the hydrophilic outer section of the bilayer in contact with water (t_h), the thickness of the hydrophobic inner segment of the bilayer (t_t) containing PBO and βCD and the respective electron densities of the solvent, outer and inner sections of the bilayer. The electron density of water (333 e^-/nm^3) was kept fixed during the fitting procedures and the determined adjustable parameters (particularly the thickness of the hydrophobic segment) are discussed hereafter. The SAXS profile reported for βCD-$(PBO_6$-$PGL_{14})_{14}$ (Trace a in

Figure 2B) on the other hand is not compatible with the vesicular morphology and it suggests the formation of small spherical micelles due to the typical Guinier plateau of the intensity at low q-values, namely, $q \leq 0.4$ nm^{-1}. Accordingly, the pattern in such a case could be properly fitted only by using the form factor for core-shell structures having the radius of the core and thickness of the shell as adjustable parameters, along with the respective electron densities.

The structural features of the self-assemblies as determined by light scattering measurements as well as the morphologies concluded based on SAXS profiles and respective fitting curves are gathered in Table 2 according to w_{PGL} value.

Table 2. Light scattering data for self-assemblies of βCD-(PBO$_m$-PGL$_n$)$_{14}$ according to the weight fraction of PGL (w_{PGL}).

Entry[a]	w_{PGL}[a]	R_H[b] (nm)	PDI[b]	Mw$_{NPs}$[c] (kDa)	Nagg[c]	Morphology
βCD-(PBO$_{30}$-PGL$_4$)$_{14}$	0.11	--[d]				Ill-aggregates
βCD-(PBO$_{24}$-PGL$_6$)$_{14}$	0.19					
βCD-(PBO$_{22}$-PGL$_7$)$_{14}$	0.23	111	0.10	4.11×10^4	1320	Polymersomes
βCD-(PBO$_{13}$-PGL$_6$)$_{14}$	0.28	90	0.10	2.96×10^4	1450	
βCD-(PBO$_7$-PGL$_5$)$_{14}$	0.35	84	0.16	5.40×10^4	3880	
βCD-(PBO$_8$-PGL$_{12}$)$_{14}$	0.57	7.7	0.28	2.06×10^2	9.29	Spherical micelles
βCD-(PBO$_6$-PGL$_{14}$)$_{14}$	0.62	5.6	0.24	1.61×10^2	7.27	

[a]Polymer formula and w_{PGL} are reported as theoretical values; [b]The hydrodynamic radius (R_H) and polydispersity indexes (PDI) are reported as the mean Z-average radius and PDI value based on 5 measurements; [c]The molecular weight of the self-assemblies (Mw$_{NPs}$) were determined using the Debye plot and the aggregation number (Nagg) was calculated using Equation 1; [d]Both DLS and SLS were unsuitable to provide the relevant parameters in these cases as explained in the main text.

The results indicate that the self-assembled morphology of βCD-(PBO-PGL)$_{14}$ is greatly dependent on w_{PGL}, reasonably obeying the phase diagram for self-assembled amphiphilic block copolymers in aqueous solution [47]. More specifically, when $w_{PGL} \leq 0.19$, the copolymers precipitated in water; when $0.23 \leq w_{PGL} \leq 0.35$, they self-assembled into polymersomes; and when $w_{PGL} \geq 0.57$, they formed spherical micelles. It is worth mentioning that these w_{PGL} ranges fit with those of linear analogues (Scheme S1, SI), demonstrating the chemical similarity between βCD-(PBO-PGL)$_{14}$ and PGL-PBO-PGL, and suggesting a low contribution of

copolymer architecture to the phase diagram when a cyclodextrin is used as central core of the star copolymer.

The stretching state of PBO chains in the polymersomes is discussed based on the relationship between membrane thickness and *X*n of PBO [48]. It is also noticed that the rigid βCD moiety contributes partly to the hydrophobic thickness, hence, the thickness attributed merely to PBO segment (t_{PBO}) was calculated as the difference between t_t and H_{CD}, *i.e.*, $t_{PBO} = t_t - H_{CD}$, with t_t being the hydrophobic thickness derived from SAXS characterization (Table S6, SI) and H_{CD} the βCD thickness taken as 0.78 nm [49] (Scheme S2, SI).

Figure 3 displays the log-log plot of t_{PBO} versus *X*n of PBO, producing a slope equal to 0.72 (blue dashed line). The membrane thickness of polymersomes made from PGL-PBO-PGL triblock copolymers ($t_{PBO} = t_t$, Table S6, SI) was also plotted as a function of *X*n of PBO revealing a slope of 0.64 (red solid line) consistent with reported results [1,48,50]. The values reflect the conformation of the chains. The upper limit of 1.0 would suggest completely stretched chains, whereas 0.5 would reflect non-perturbed state of the chains (Gaussian like) in the membrane. The values are close to 2/3 in agreement with the classical strong segregation theory and they suggest that PBO chains are to some extent slightly more stretched in the produced membranes using the star copolymers. Presumably, the βCD-cored architecture induces a lateral crowding environment and respectively, the stretching of the PBO segment [51]. Nevertheless, overall the star copolymers (blue dots) are scattered aside the master curve of the linear copolymers (red line) thus suggesting that the conformation and stretching state of PBO segments are reasonably similar. These data along with the aforementioned chemical features permit to investigate the influence of the βCD cavity on the permeability of the membranes made using βCD-(PBO-PGL)$_{14}$ as compared with the behavior of linear triblock copolymer counterparts.

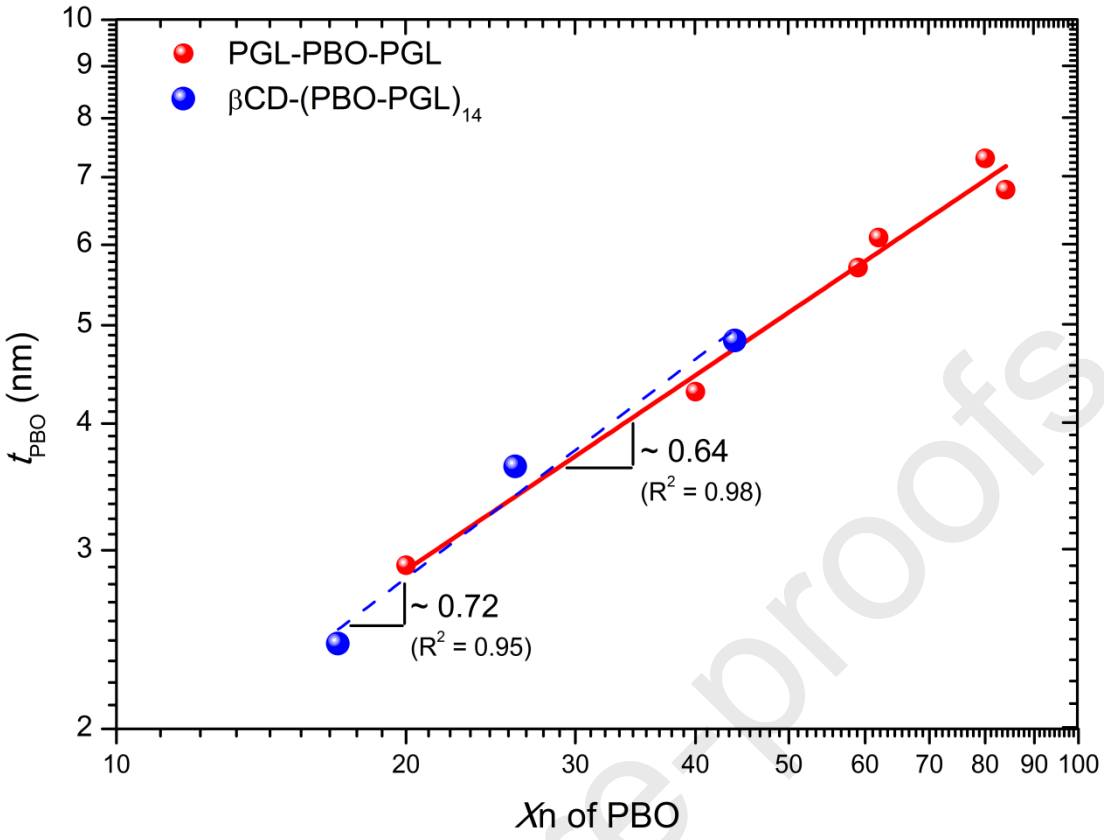

Figure 3. Master curves plotting the thickness of PBO segment (t_{PBO}) as a function of the degree of polymerization of PBO (*X*n of PBO), in the contexts of the polymersomes made using βCD-(PBO-PGL)$_{14}$ (blue) and PGL-PBO-PGL (red). The values are the slope and coefficient of determination (R^2) of respective fitting curves.

3.3. Polymersome permeability to H^+

The investigation on the polymersome permeability to H^+ was performed by adding HCl outside the polymersomes and monitoring the changes in the inner pH of the vesicles induced by proton diffusion. To this end, the fluorescent probe 8-hydroxypyrene-1,3,6-trisulfonic acid trisodium salt (HPTS) was used to determine the inner pH of polymersomes (pH_f) because the probe is water-soluble and membrane impermeable, and the ratiometric assay provides good accuracy to the pH measurement [34,52]. In the present work, HPTS was loaded exclusively inside polymersomes by rehydrating polymer thin film with HPTS solution followed with extensive dialysis, producing the HPTS-loaded vesicles (HPTS-pos). The fluorescent polymersomes (HPTS-pos) were then applied to study the membrane permeability to H^+.

Figure 4 provides the plots of pH_f as a function of time. Each panel displays the reduction in polymersome inner pH in the HPTS-pos sample (red filled symbol) and of the pH value in a HPTS solution (control experiment, black open symbol). All the curves provide a similar decaying trend nevertheless, in HPTS solutions (black open symbols) pH_f decays gradually and stops decreasing after roughly 10 minutes of HCl addition, while it takes more time for pH_f to reach the plateau in HPTS-pos solutions (red filled symbols). pH_f decays slower in the presence of polymersomes, implying polymersome membrane retards proton influx to some extent. In this regard, the thickness, copolymer architecture and the presence of βCD may influence proton diffusion. To investigate this issue, the experimental profiles were analyzed quantitatively.

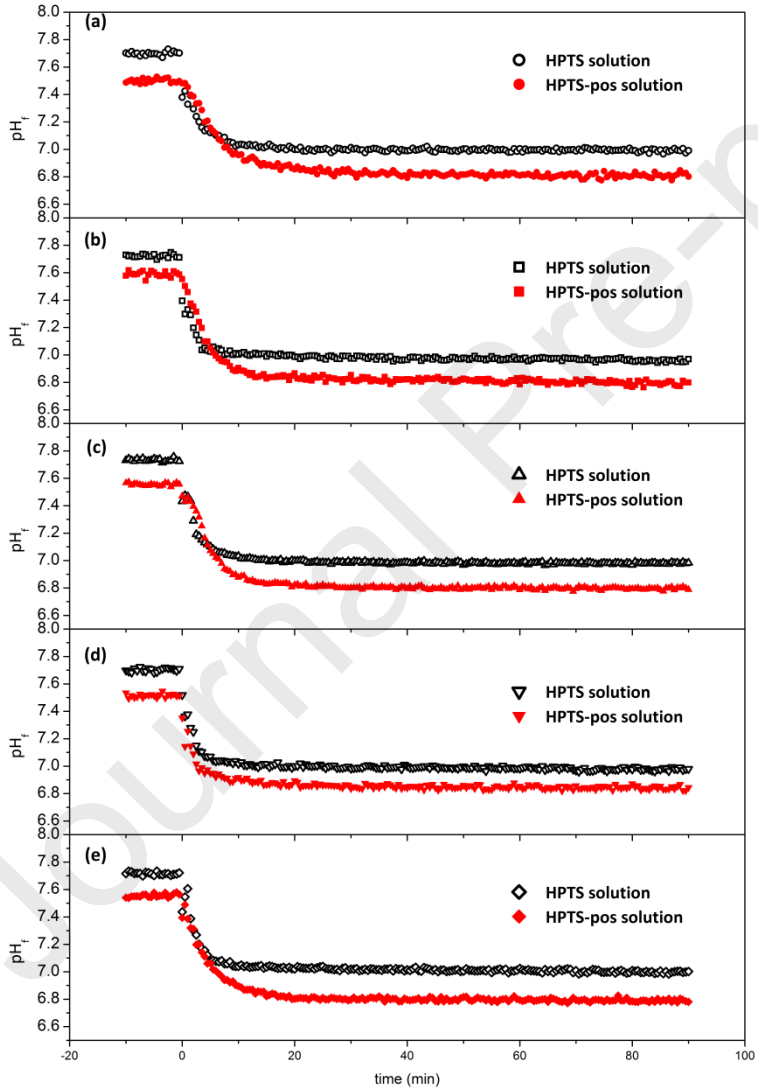

Figure 4. Stacked pH_f decaying plots, in HPTS-pos solutions (red filled symbols) of (a) PGL_{25}-PBO_{80}-PGL_{25}, (b) PGL_{21}-PBO_{84}-PGL_{21}, (c) PGL_{18}-PBO_{62}-PGL_{18}, (d) PGL_6-PBO_{40}-PGL_6, and (e) βCD-$(PBO_{13}$-$PGL_6)_{14}$, as well as in respective HPTS solutions (black open symbols).

The decay time parameter (τ) was obtained by fitting the pH_f decaying curve into the exponential decay function (Equation 3) [53]:

$$pH_f = Ae^{(-t/\tau)} + pH_{f0} \quad (3)$$

where pH_f is the pH value derived from fluorospectrometry, either the inner pH of the polymersomes in HPTS-pos solution or the pH value of HPTS solution, and t is time, both are experimental values. A, τ and pH_{f0} are the fitting parameters. The fitting results were gathered in Table 3 according to the hydrophobic thickness of the polymersomes (t_t).

Table 3. Fitting parameters of the pH_f decaying plots of different polymersomes, according to the thickness of the hydrophobic layer (t_t)[a].

Entry	Polymer	t_t[a] (nm)	HPTS solution		HPTS-pos solution		$\Delta\tau$[b] (min)
			τ_{blank} (min)	R^2	τ_{pos} (min)	R^2	
a	PGL_{25}-PBO_{80}-PGL_{25}	7.3	3.65	0.9541	6.51	0.9755	2.87
b	PGL_{21}-PBO_{84}-PGL_{21}	6.8	2.37	0.9122	5.07	0.9381	2.70
c	PGL_{18}-PBO_{62}-PGL_{18}	6.1	3.23	0.9676	5.29	0.9798	2.06
d	PGL_6-PBO_{40}-PGL_6	4.3	2.38	0.9535	2.99	0.9244	0.61
e	βCD-$(PBO_{13}$-$PGL_6)_{14}$	4.4	3.14	0.9399	5.21	0.9837	2.07

[a]thickness of the hydrophobic layer of the polymersomes (t_t) as determined by SAXS; [b]time-lag ($\Delta\tau$) as the decay time difference between HPTS-pos and HPTS ($\Delta\tau = \tau_{pos} - \tau_{blank}$).

In each pair of HPTS-pos and HPTS reference solutions, the τ value of HPTS-pos suspension (τ_{pos}) is larger than the one of HPTS solution (τ_{blank}). Accordingly, the difference, *i.e.* $\Delta\tau = \tau_{pos} - \tau_{blank}$, indicates the time-lag issued from the presence of polymersome membrane. One might notice that τ_{blank} slightly varies from one experiment to another. This is possibly due to the varied HPTS concentrations (Table S7) and/or experimental temperature (experiments were conducted at room temperature). The potential influence of HPTS concentration was minimized by performing the respective control experiment with a HPTS solution having the same HPTS concentration as that in the HPTS-pos suspension (Table S7). One experiment lasted about 2 hours, thus the experiment with HPTS-pos suspension and its control experiment were performed sequentially so as to minimize the potential influence of temperature. In this way, the time lag ($\Delta\tau$), correspondingly the membrane

permeability, is thought to mainly depend on the characteristics of polymersomes, such as the hydrophobic thickness [34,54] and the chemical composition [55].

The influence of hydrophobic thickness was assayed by comparing the results from the polymersome made using linear amphiphilic copolymers. The data indicates that $\Delta\tau$ decreased by reducing t_t (Table 3, Entries a−d). In other words, proton diffused faster through thinner PGL-PBO-PGL membranes. This result agrees with the reported results concerning the OH^- permeability of poly(ethylene oxide)-*block*-polybutadiene (PEO-PBD) membranes [34].

The influence of the presence of βCD was probed by the proton permeability of the vesicles made from βCD-$(PBO_{13}$-$PGL_6)_{14}$. The pH_f decaying plots of βCD-$(PBO_{13}$-$PGL_6)_{14}$ polymersomes and HPTS solutions (Figure 4e) have the same trends as those of PGL-PBO-PGL (Figure 4a−d). Compared to PGL_6-PBO_{40}-PGL_6, βCD-$(PBO_{13}$-$PGL_6)_{14}$ counterparts have a comparable hydrophobic thickness but larger $\Delta\tau$ was monitored. This result is unexpected to some extent since βCD and its derivatives have been reported to increase the permeability of various types of membranes to various permeants thanks to its rigid hollow structure [22−25,27−29]. Moreover, the PBO chains in the polymersome membrane made from βCD-cored star copolymers were slightly more stretched than those in the membranes produced from linear copolymers. Although the volume occupied by the cyclodextrins in the hydrophobic part of the βCD-$(PBO_{13}$-$PGL_6)_{14}$ membrane is small (~1% *v/v*), the formation of a thin layer of βCD acting as a proton trap, the introduction of complexity in the hydrophobic segment, the attenuation of the ionic conductivity of the material and/or more specific events that have to be investigated to explain the slower proton diffusion. However, these hypotheses remain to be confirmed. Additionally, the exact inner structure of the hydrophobic layer has to be elucidated in order to be correlated with such hypotheses.

3.4. Planar polymer membrane permeability to K^+Cl^-

The effect of the βCD cavity on the permeability of polymeric membranes to K^+Cl^- was further probed using the black lipid membrane (BLM) technique. To this end, the planar polymeric membrane of linear or star copolymers was painted in a 150-µm window separating two chambers, which were filled with a 1 M KCl solution. Figures 5 and 6 display representative plots of current intensity as a function of time which were recorded under constant voltage, for linear and star copolymer membranes respectively.

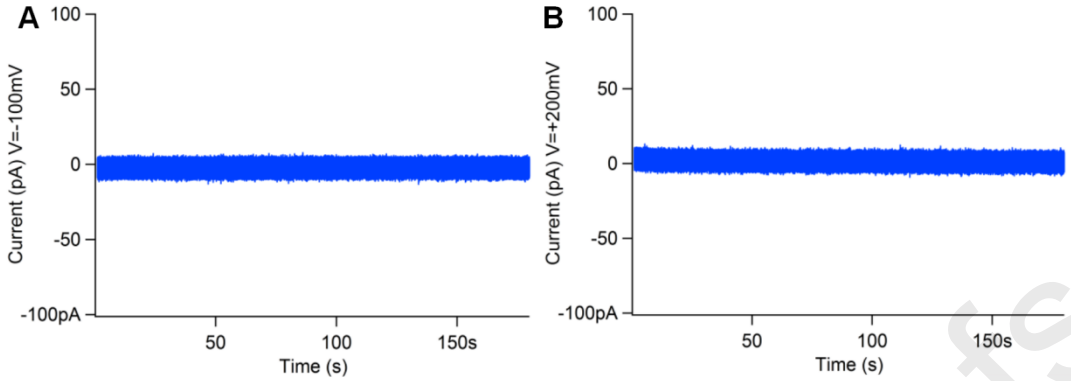

Figure 5. Representative current intensity plots as a function of time (zoom of 3 minutes of an experiment run during 30 minutes) with applied voltage of (A) -100 mV and (B) +200 mV, for PGL_8-PBO_{42}-PGL_8 membrane. The experiments were repeated four times.

Figure 5A and B portray the typical records of current intensity versus time obtained with planar PGL_8-PBO_{42}-PGL_8 membrane when -100 mV and +200 mV tension are applied, respectively. The recorded intensity versus time is constant up to 30 minutes, at a value close to 0 pA, when the applied voltage was set to -100 mV or +200 mV on the same membrane. These results, indeed highly reproducible (at least 4 membranes tested), strongly support that the PGL_8-PBO_{42}-PGL_8 membrane is insulating, impermeable to K^+Cl^-. It has to be noticed that PGL_8-PBO_{42}-PGL_8 membranes are more stable than lipid membranes, which tend to collapse at voltages higher than +/-100 mV [2,56,57]. Three other linear copolymers were tested (PGL_8-PBO_{59}-PBO_8, PGL_{10}-PBO_{49}-PGL_{10} and PGL_9-PBO_{33}-PGL_9) with the voltage of -100 mV and +200 mV. In each case, the electrical trace showed an intensity versus time equal to 0 pA, typical results for impermeable membranes.

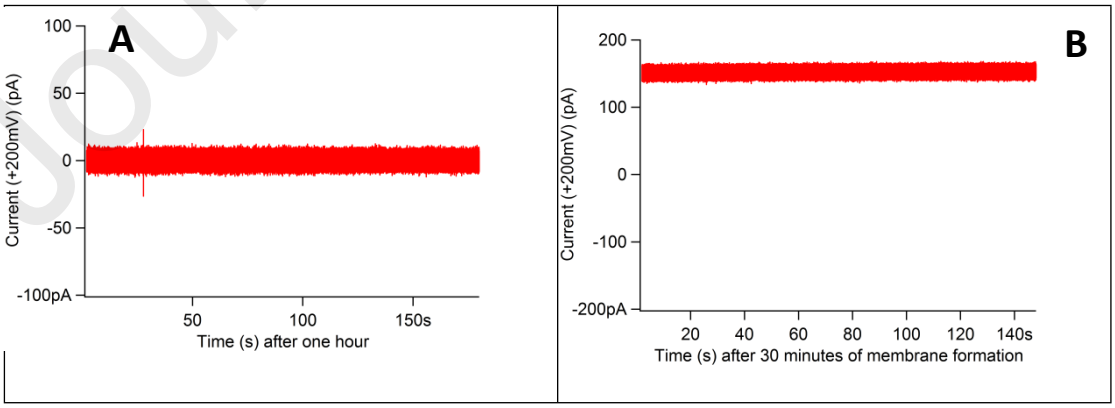

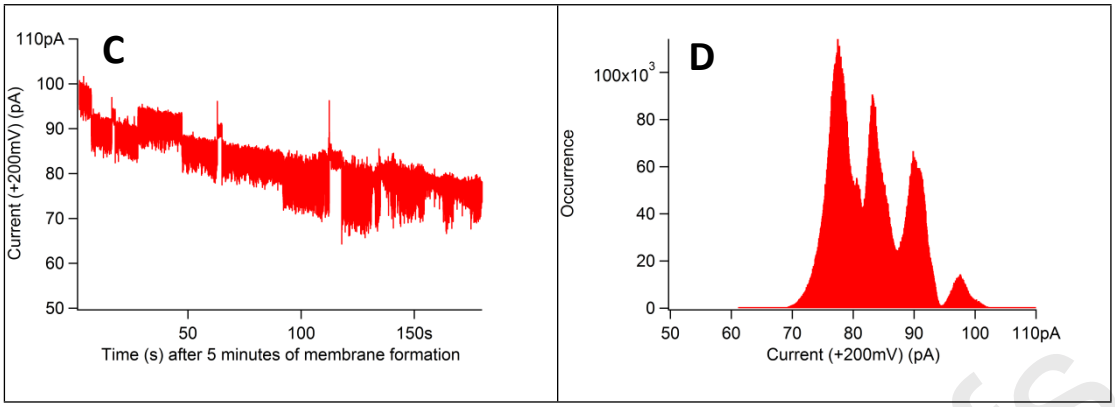

Figure 6. Representative **c**urrent intensity plots as a function of time (zoom of 3 minutes of an experiment run during one hour) with applied voltage of +200 mV, for βCD-$(PBO_{13}$-$PGL_6)_{14}$ membrane (A,B,C) and (D) the corresponding occurrence histogram of (C), based on 12 experiments.

Figure 6 displays a typical set of BLM results obtained for βCD-$(PBO_{13}$-$PGL_6)_{14}$ membranes. Figure 6A shows a recorded intensity versus time constant after one hour, at a value close to 0 pA, when the applied voltage was set to +200 mV. These results strongly support that the membrane acts as an insulator and is impermeable to K^+Cl^-. Six membranes out of 12 attempts had an insulating behavior for K^+ and Cl^- (Figure 6A). However, considering 6 other attempts, porosity could be observed and two typical behaviors could be evidenced. Figure 6B displays typical records of intensity as a function of time observed for 4 different membranes. The positive value of the intensity when a positive voltage is applied suggests the formation of a stable porous membrane: ion transfer through the membrane was obtained from the beginning of the record (the intensity gets negative when a negative tension is applied, on the same membrane). The last two attempts (Figure 6C) provided intensity versus time records with discrete current jumps. One can notice that the obtained current jumps are in the same range as those reported in the literature where βCD-cored star copolymers were inserted in lipid bilayers [24,25]. The histogram of occurrence of the events (Figure 6D), resulting from the analysis of the electrical traces, shows the tendency of ion transfer through well-defined structures, the difference between the currents being reproducible. Since no event could be evidenced for CD-free triblock PGL-PBO-PGL, the presence of βCD cavity in βCD-$(PBO_{13}$-$PGL_6)_{14}$-based membrane has an influence on the polymer membrane permeabilization and could induce porosity on the planar membrane made from βCD-cored star copolymers. The mechanism that permits the permeabilization of βCD-$(PBO_{13}$-$PGL_6)_{14}$ membrane cannot be deciphered from the BLM measurements. A random permeabilization of the βCD-$(PBO_{13}$-$PGL_6)_{14}$ membrane is observed for the set of investigated membranes and more work will be devoted to strengthen the control of βCD-$(PBO_{13}$-$PGL_6)_{14}$ membrane permeation to K^+ and Cl^- ions.

Conclusions

The present work aimed to optimize and synthesize a library of 14-armed star block copolymers comprising hydrophobic (PBO) and hydrophilic (PGL) segments, and to assess the self-assembly behavior and the ion permeability. In a wider scope, we are targeting the preparation manufacturing of polymeric vesicles containing functional nanochannels. Hydrophilic-to-hydrophobic weight ratio must be precisely tuned to reach the desired morphology (hollow spheres). We presently succeeded to produce a variety of βCD-cored star amphiphilic copolymers (βCD-(PBO-PGL)$_{14}$) having low polydispersity, high purity and tailor-made block lengths. The self-assembly behavior was subsequently studied and we were able to engineer well-defined polymeric vesicles as confirmed by light scattering and SAXS measurements. Interestingly, despite the tiny differences observed regarding the conformation and stretching state of PBO segments, the βCD-(PBO-PGL)$_{14}$ self-assembly behavior in aqueous solution is close to the one of the linear analogues PGL-PBO-PGL. The βCD-containing vesicles were evidenced to be less permeable to protons compared to the linear counterparts. Linear block copolymer planar membranes were impermeable to K^+ and Cl^-, while the ones produced from βCD-(PBO-PGL)$_{14}$ were not. Accordingly, these data evidence that the presence of βCD in the structure of the assemblies influences the permeability of polymeric membranes to some extent. Truly, although behaving slightly different in the kinetic point of view, we demonstrated that both types of polymeric vesicles (either containing or not β-CD) are intrinsically permeable to protons and can therefore be thought as potential candidates for instance in the designing of nano-factories towards applications where precise changes in environmental pH are required. As a vision of future work, we are making efforts to tune polymer membrane permeability by adjusting the composition of the membrane-forming polymers. Additionally, there are investigations underway where the passive exchange of small molecules of different sizes and chemical nature is being investigated.

Acknowledgments

H.D. acknowledges the Ph.D. scholarship offered by the China Scholarship Council (CSC). FCG acknowledges the financial support provided by FAPESP (Grants 2019/06634-8 and 2021/12071-6). The authors acknowledge the SOLEIL synchrotron for allocation of synchrotron beamtime on the SWING beamline and Aurélien Thureau for his technical assistance.

References

1. Le Meins J F, Sandre O, Lecommandoux S. Recent trends in the tuning of polymersomes' membrane properties. The European Physical Journal E, 2011, 34(2): 1-17.

2. Rideau E, Dimova R, Schwille P, et al. Liposomes and polymersomes: a comparative review towards cell mimicking. Chemical society reviews, 2018, 47(23): 8572-8610.

3. Dao T P T, Brûlet A, Fernandes F, et al. Mixing block copolymers with phospholipids at the nanoscale: from hybrid polymer/lipid wormlike micelles to vesicles presenting lipid nanodomains. Langmuir, 2017, 33(7): 1705-1715.

4. Vance J A, Devaraj N K. Membrane Mimetic Chemistry in Artificial Cells. Journal of the American Chemical Society, 2021.

5. Iqbal S, Blenner M, Alexander-Bryant A, et al. Polymersomes for therapeutic delivery of protein and nucleic acid macromolecules: from design to therapeutic applications. Biomacromolecules, 2020, 21(4): 1327-1350.

6. Zhu Y, Yang B, Chen S, et al. Polymer vesicles: Mechanism, preparation, application, and responsive behavior. Progress in Polymer Science, 2017, 64: 1-22.

7. Zartner L, Muthwill M S, Dinu I A, et al. The rise of bio-inspired polymer compartments responding to pathology-related signals. Journal of Materials Chemistry B, 2020, 8(29): 6252-6270.

8. Che H, van Hest J C M. Adaptive polymersome nanoreactors. ChemNanoMat, 2019, 5(9): 1092-1109.

9. Chen Q, Schönherr H, Vancso G J. Block-Copolymer Vesicles as Nanoreactors for Enzymatic Reactions. Small, 2009, 5(12): 1436-1445.

10. Baumann P, Spulber M, Fischer O, et al. Investigation of Horseradish Peroxidase Kinetics in an "Organelle-Like" Environment. Small, 2017, 13(17): 1603943.

11. Einfalt T, Witzigmann D, Edlinger C, et al. Biomimetic artificial organelles with in vitro and in vivo activity triggered by reduction in microenvironment. Nature communications, 2018, 9(1): 1-12.

12. Discher D E, Ahmed F. Polymersomes. Annu. Rev. Biomed. Eng., 2006, 8: 323-341.

13. LoPresti C, Lomas H, Massignani M, et al. Polymersomes: nature inspired nanometer sized compartments. Journal of Materials Chemistry, 2009, 19(22):

3576-3590.

14. Palivan C G, Goers R, Najer A, et al. Bioinspired polymer vesicles and membranes for biological and medical applications. Chemical society reviews, 2016, 45(2): 377-411.

15. Alexandridis P, Lindman B. Amphiphilic block copolymers: self-assembly and applications. Elsevier, 2000.

16. Blackman L D, Varlas S, Arno M C, et al. Permeable protein-loaded polymersome cascade nanoreactors by polymerization-induced self-assembly. ACS macro letters, 2017, 6(11): 1263-1267.

17. Bleul R, Thiermann R, Maskos M. Techniques to control polymersome size. Macromolecules, 2015, 48(20): 7396-7409.

18. Meier W, Nardin C, Winterhalter M. Reconstitution of channel proteins in (polymerized) ABA triblock copolymer membranes. Angewandte Chemie International Edition, 2000, 39(24): 4599-4602.

19. Zheng S, Huang L, Sun Z, et al. Self-assembled artificial ion-channels toward natural selection of functions. Angewandte Chemie International Edition, 2021, 60(2): 566-597.

20. Tabushi I, Kuroda Y, Yokota K. A, B, D, F-tetrasubstituted β-cyclodextrin as artificial channel compound. Tetrahedron Letters, 1982, 23(44): 4601-4604.

21. Khan A R, Forgo P, Stine K J, et al. Methods for selective modifications of cyclodextrins. Chemical Reviews, 1998, 98(5): 1977-1996.

22. Badi N, Auvray L, Guégan P. Synthesis of Half-Channels by the Anionic Polymerization of Ethylene Oxide Initiated by Modified Cyclodextrin. Advanced Materials, 2009, 21(40): 4054-4057.

23. El Ghoul Y, Renia R, Faye I, et al. Biomimetic artificial ion channels based on beta-cyclodextrin. Chemical Communications, 2013, 49(99): 11647-11649.

24. Eskandani Z, Le Gall T, Montier T, et al. Polynucleotide transport through lipid membrane in the presence of starburst cyclodextrin-based poly (ethylene glycol)s. The European Physical Journal E, 2018, 41(11): 1-7.

25. Faye I, Huin C, Illy N, et al. β-Cyclodextrin-Based Star Amphiphilic Copolymers: Synthesis, Characterization, and Evaluation as Artificial Channels. Macromolecular Chemistry and Physics, 2019, 220(2): 1800308.

26. Ravoo B J, Darcy R. Cyclodextrin bilayer vesicles. Angewandte Chemie, 2000, 112(23): 4494-4496.

27. Himmelein S, Sporenberg N, Schönhoff M, et al. Size-selective permeation of water-soluble polymers through the bilayer membrane of cyclodextrin vesicles investigated by PFG-NMR. Langmuir, 2014, 30(14): 3988-3995.

28. Liu J, Xiao Y, Liao K S, et al. Highly permeable and aging resistant 3D architecture from polymers of intrinsic microporosity incorporated with beta-cyclodextrin. Journal of Membrane Science, 2017, 523: 92-102.

29. Tang Y J, Shen B J, Huang B Q, et al. High permselectivity thin-film composite nanofiltration membranes with 3D microstructure fabricated by incorporation of beta cyclodextrin. Separation and Purification Technology, 2019, 227: 115718.

30. Nichols J W, Abercrombie R F. A view of hydrogen/hydroxide flux across lipid membranes. The Journal of membrane biology, 2010, 237(1): 21-30.

31. Clausen M J V, Poulsen H. Sodium/potassium homeostasis in the cell. Metallomics and the Cell. Springer, Dordrecht, 2013: 41-67.

32. Taton D, Borgne AL, Sepulchre M, et al. Synthesis of chiral and racemic functional polymers from glycidol and thioglycidol. Macromolecular Chemistry and Physics, 1994, 195: 139-148

33. Du H, de Oliveira F A, Albuquerque L J C, et al. Polyglycidol-Stabilized Nanoparticles as a Promising Alternative to Nanoparticle PEGylation: Polymer Synthesis and Protein Fouling Considerations. Langmuir, 2020, 36(5): 1266-1278.

34. Paxton W F, Price D, Richardson N J. Hydroxide ion flux and pH-gradient driven ester hydrolysis in polymer vesicle reactors. Soft Matter, 2013, 9(47): 11295-11302.

35. Parnell A J, Tzokova N, Topham P D, et al. The efficiency of encapsulation within surface rehydrated polymersomes. Faraday discussions, 2009, 143: 29-46.

36. Hope M J, Bally M B, Webb G, et al. Production of large unilamellar vesicles by a rapid extrusion procedure. Characterization of size distribution, trapped volume and ability to maintain a membrane potential. Biochimica et Biophysica Acta (BBA)-Biomembranes, 1985, 812(1): 55-65.

37. Nardin C, Hirt T, Leukel J, et al. Polymerized ABA triblock copolymer vesicles. Langmuir, 2000, 16(3): 1035-1041.

38. Eskandani Z, Huin C, Guégan P. Regioselective allylation of cyclomaltoheptaose (β-cyclodextrin) leading to per(2,6-di-O-hydroxypropyl-3-O-methyl)-β-cyclodextrin. Carbohydrate research, 2011, 346(15): 2414-2420.

39. Huin C, Eskandani Z, Badi N, et al. Anionic ring-opening polymerization of ethylene oxide in DMF with cyclodextrin derivatives as new initiators. Carbohydrate polymers, 2013, 94(1): 323-331.

40. Isono T, Kamoshida K, Satoh Y, et al. Synthesis of star-and figure-eight-shaped polyethers by t-Bu-P4-catalyzed ring-opening polymerization of butylene oxide. Macromolecules, 2013, 46(10): 3841-3849.

41. Misaka H, Tamura E, Makiguchi K, et al. Synthesis of end-functionalized polyethers by phosphazene base-catalyzed ring-opening polymerization of 1, 2-butylene oxide and glycidyl ether. Journal of Polymer Science Part A: Polymer Chemistry, 2012, 50(10): 1941-1952.

42. Lee B F, Wolffs M, Delaney K T, et al. Reactivity ratios and mechanistic insight for anionic ring-opening copolymerization of epoxides. Macromolecules, 2012, 45(9): 3722-3731.

43. Puchelle V, Du H, Illy N, et al. Polymerization of epoxide monomers promoted by *t*BuP$_4$ phosphazene base: a comparative study of kinetic behavior. Polymer Chemistry, 2020, 11(21): 3585-3592.

44. Hans M, Keul H, Moeller M. Chain transfer reactions limit the molecular weight of polyglycidol prepared via alkali metal based initiating systems. Polymer, 2009, 50(5): 1103-1108.

45. Gervais M, Brocas A L, Cendejas G, et al. Synthesis of linear high molar mass glycidol-based polymers by monomer-activated anionic polymerization. Macromolecules, 2010, 43(4): 1778-1784.

46. Kamata Y, Parnell A J, Gutfreund P, et al. Hydration and ordering of lamellar block copolymer films under controlled water vapor. Macromolecules, 2014, 47(24): 8682-8690.

47. Blanazs A, Armes S P, Ryan A J. Self-assembled block copolymer aggregates: from micelles to vesicles and their biological applications. Macromolecular rapid communications, 2009, 30(4−5): 267-277.

48. Battaglia G, Ryan A J. Bilayers and interdigitation in block copolymer vesicles. Journal of the American Chemical Society, 2005, 127(24): 8757-8764.

49. Van De Manakker F, Vermonden T, Van Nostrum C F, et al. Cyclodextrin-based polymeric materials: synthesis, properties, and pharmaceutical/biomedical applications. Biomacromolecules, 2009, 10(12): 3157-3175.

50. Wehr R, Gaitzsch J, Daubian D, et al. Deepening the insight into poly (butylene oxide)-block-poly (glycidol) synthesis and self-assemblies: micelles, worms and vesicles. RSC Advances, 2020, 10(38): 22701-22711.

51. Hu M, Shen Y, Zhang L, et al. Polymersomes via self-assembly of amphiphilic β-cyclodextrin-centered triarm star polymers for enhanced oral bioavailability of water-soluble chemotherapeutics. Biomacromolecules, 2016, 17(3): 1026-1039.

52. Wu J, Eisenberg A. Proton diffusion across membranes of vesicles of poly(styrene-b-acrylic acid) diblock copolymers. Journal of the American Chemical Society, 2006, 128(9): 2880-2884.

53. Schroeder T B H, Leriche G, Koyanagi T, et al. Effects of lipid tethering in extremophile-inspired membranes on H^+/OH^- flux at room temperature. Biophysical journal, 2016, 110(11): 2430-2440.

54. Battaglia G, Ryan A J, Tomas S. Polymeric vesicle permeability: a facile chemical assay. Langmuir, 2006, 22(11): 4910-4913.

55. Avnir Y, Barenholz Y. pH determination by pyranine: medium-related artifacts and their correction. Analytical biochemistry, 2005, 347(1): 34-41.

56. White S H. A study of lipid bilayer membrane stability using precise measurements of specific capacitance. Biophysical journal, 1970, 10(12): 1127-1148.

57. Seuring J, Reiss P, Koert U, et al. Synthesis, characterization and properties of a new polymerisable surfactant: 12-Methacryloyl dodecylphosphocholine. Chemistry and physics of lipids, 2010, 163(4-5): 367-372.

Supplementary Information

Engineering of Ion Permeable Planar Membranes and Polymersomes based on β-Cyclodextrin-Cored Star Copolymers

Haiqin DU[1], Sandra KALEM[1], Cécile HUIN[1,2], Nicolas ILLY[1], Guillaume TRESSET[3], Fernando Carlos GIACOMELLI[1,4], Philippe GUÉGAN[1]*

[1]Equipe Chimie des Polymères, Institut Parisien de Chimie Moléculaire (UMR-CNRS 8232), Sorbonne Université, 75252 Paris, France;

[2]Université d'Evry Val d'Essonne, Université Paris-Saclay, 91000 Evry, France

[3]Université Paris-Saclay, CNRS, Laboratoire de Physique des Solides, 91405 Orsay, France

[4]Centro de Ciências Naturais e Humanas, Universidade Federal do ABC, 09210-580 Santo André, Brazil

1. βCD-based initiator

The initiator, per(2-O-methyl-3,6-di-O-(3-hydroxypropyl))-βCD (βCD-$(OH)_{14}$) used in this work, was synthesized following a published procedure [1]. Its structure was confirmed by ^{1}H, ^{13}C and COSY spectra, as shown in Figure S1.

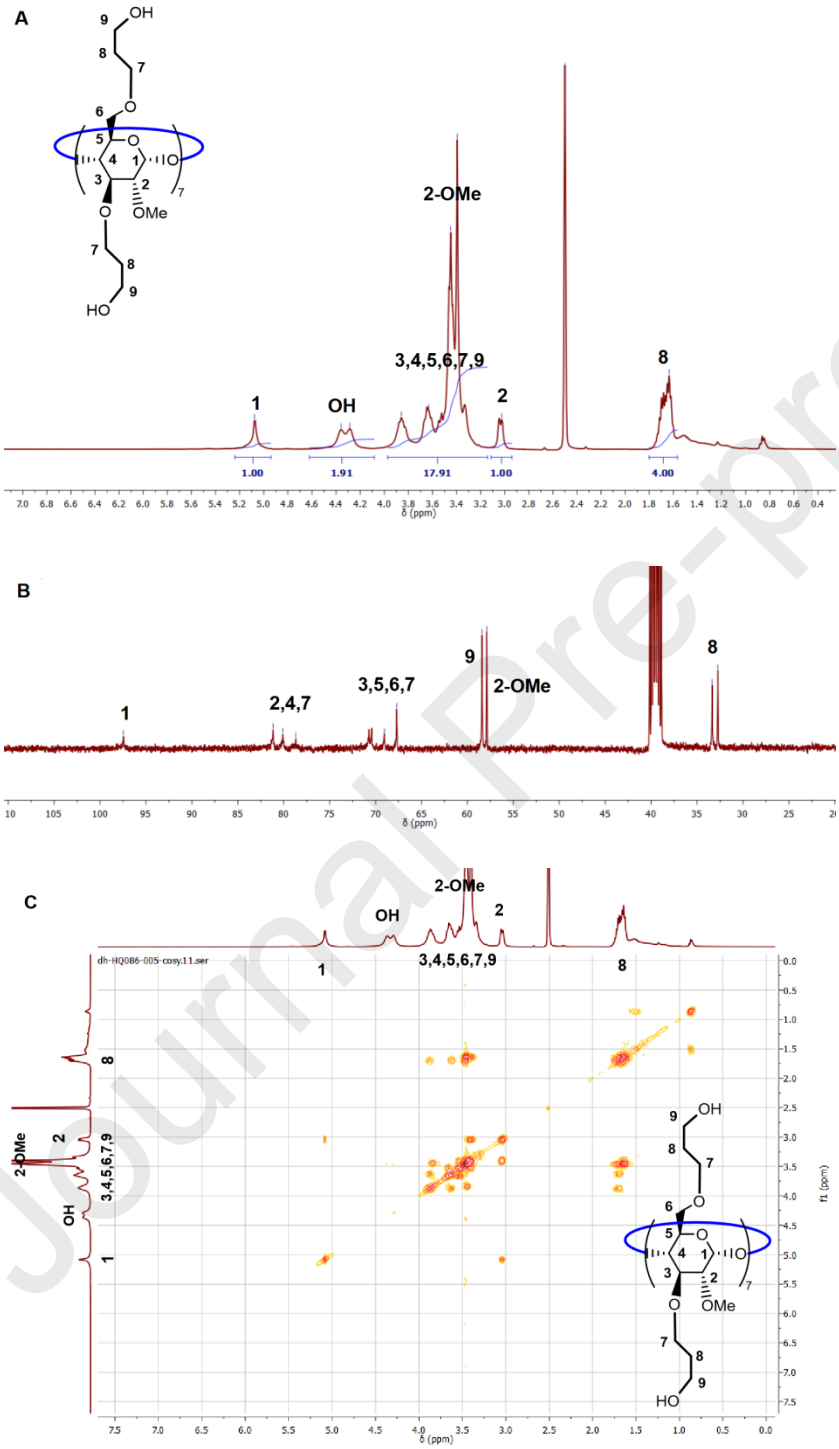

Figure S1. Representative (A) ^{1}H, (B) ^{13}C and (C) COSY NMR spectra of per(2-O-methyl-3,6-di-O-(3-hydroxypropyl))-βCD (βCD-$(OH)_{14}$), recorded in DMSO-d6 at 300 K.

2. Ethoxyethyl glycidyl ether (EEGE)

EEGE was prepared according to a published method [2]. Its structure was confirmed by ^{1}H, ^{13}C and COSY spectra, as shown in Figure S2.

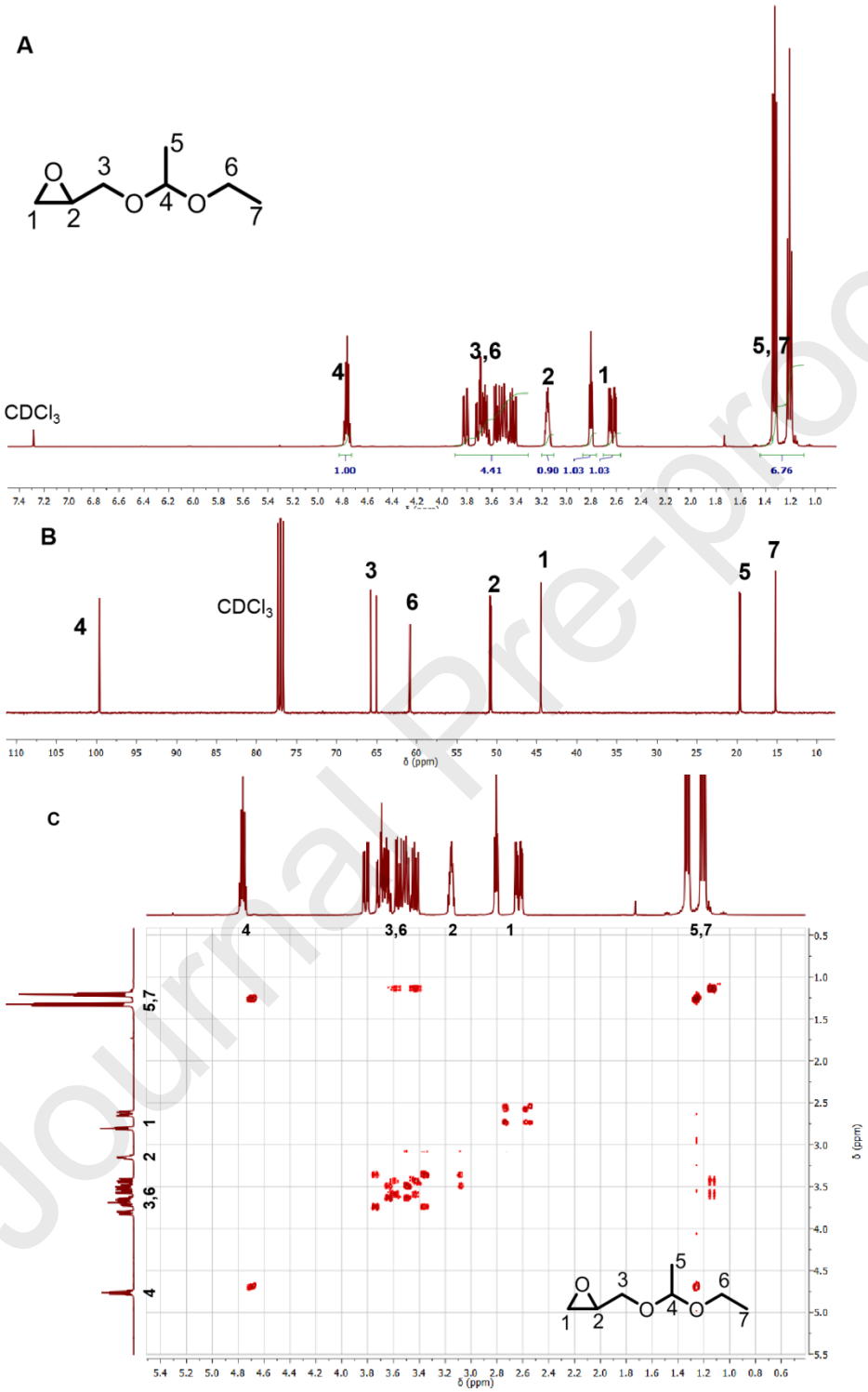

Figure S2. Representative (A) ^{1}H, (B) ^{13}C and (C) COSY NMR spectra of ethoxyethyl glycidyl ether (EEGE), recorded in $CDCl_3$, at 300 K.

3. Polyglycidol-block-poly(butylene oxide)-block-polyglycidol (PGL-PBO-PL)

The linear analogues were synthesized following the same procedure as previously reported [3]. The characteristics of the linear copolymers used for systematic study of self-assembly behavior as well as the characteristics of respective self-assemblies are listed in Table S1.

Table S1. Characteristics of PGL-PBO-PGL and respective self-assemblies according to the weight fraction of PGL (w_{PGL}).

Polymer[a]	w_{PGL}[a]	$M_{n,SEC}$[b] (kg mol^{-1})	$Đ$[b]	R_H[c] (nm)	PDI[c]	$M_{w,NPs}$[d] (kDa)	N_{agg}[d]	Morphology
PGL_7-PBO_{84}-PGL_7	0.14	8.3	1.08	--[e]				Ill-aggregates
PGL_{10}-PBO_{81}-PGL_{10}	0.19	10.6	1.03					
PGL_{11}-PBO_{85}-PGL_{11}	0.21	8.6	1.07					
PGL_{12}-PBO_{84}-PGL_{12}	0.22	8.7	1.10	124	0.12	9.71×10^4	12100	Polymersomes
PGL_6-PBO_{40}-PGL_6	0.23	5.4	1.07	109	0.10	6.17×10^4	15800	
PGL_{21}-PBO_{84}-PGL_{21}	0.33	10.1	1.09	111	0.18	7.64×10^4	8300	
PGL_6-PBO_{20}-PGL_6	0.35	3.6	1.09	87.8	0.21	1.61×10^5	67200	
PGL_{18}-PBO_{62}-PGL_{18}	0.37	10.1	1.05	133	0.20	3.76×10^4	5150	
PGL_{25}-PBO_{80}-PGL_{25}	0.39	9.2	1.19	89.7	0.08	8.30×10^4	8640	
PGL_{20}-PBO_{59}-PGL_{20}	0.40	9.9	1.05	79.5	0.10	6.48×10^4	8760	
PGL_{16}-PBO_{41}-PGL_{16}	0.43	7.6	1.08	83.3	0.21	3.07×10^4	4040	Cylindrical Micelles
PGL_7-PBO_{14}-PGL_7	0.46	3.1	1.12	11.3	0.19	7.58×10^2	361	Spherical Micelles
PGL_{10}-PBO_{21}-PGL_{10}	0.47	4.9	1.09	20.5	0.21	4.60×10^3	933	
PGL_{22}-PBO_{13}-PGL_{22}	0.75	5.9	1.14	13.4	0.21	6.68×10^2	155	

[a]The formula and w_{PGL} of polymers are reported as theoretical values; [b]Molar mass ($M_{n,SEC}$) and polydispersity index of polymer ($Đ$) are reported as the SEC characterization results, with PMMA as the standard and using a RI detector; [c]Hydrodynamic radius (R_H) and polydispersity index (PDI) of self-assemblies were determined by DLS and reported as mean values of 5 measurements; [d]Molecular weight ($M_{w,NPs}$) and number of aggregation (N_{agg}) were determined by SLS using the Debye plot; [e]Morphology was assigned based on DLS, SLS, SAXS and TEM characterization with details referring to our previous work [3]; [e]No data because the undefined aggregates were unsuitable for DLS and SLS measurements.

4. pH calibration curve for determination of vesicular interior pH value

The pH calibration curve was constructed following a published protocol [4]. Typically, a set of phosphate buffering (PB) solutions of varied pH values was prepared, by adjusting the pH value of NaH_2PO_4 solution (25 mM) with NaOH solution (1 M) or 0.5 M H_3PO_4 solution (0.5 M) to the desired pH. Then, a set of working solutions of HPTS was prepared by diluting a stock solution (1.0 mg mL^{-1} in H_2O) to the concentration of 1.0 μg mL^{-1} with PB. The pH values of working solutions were measured using a pH meter. Subsequently, the fluorescence excitation spectra of the working solutions were recorded on a Cary Eclipse fluorophotometer at room temperature., with λ_{em} 509 nm and both ex-slit and em slit 2.5 nm. For each working solution, the spectrum was recorded 5 times. At last, the intensity ratios of I_{455}/I_{402} and pH values were fitted into the Henderson−Hasselbalch relation (Equation 1) to construct the pH calibration curve [4,5].

$$pH = \frac{A3 - \log(\frac{A2 - r}{r - A1})}{A4} \quad (1)$$

wherein r is the intensity ratio of I_{455}/I_{402}, pH is the pH value measured by electronic pH meter and the constants $A1$, $A2$, $A3$, and $A4$ are fitting parameters.

The representative calibration curve is portrayed in Figure S3, producing comparable fitting parameters to the reported values [4].

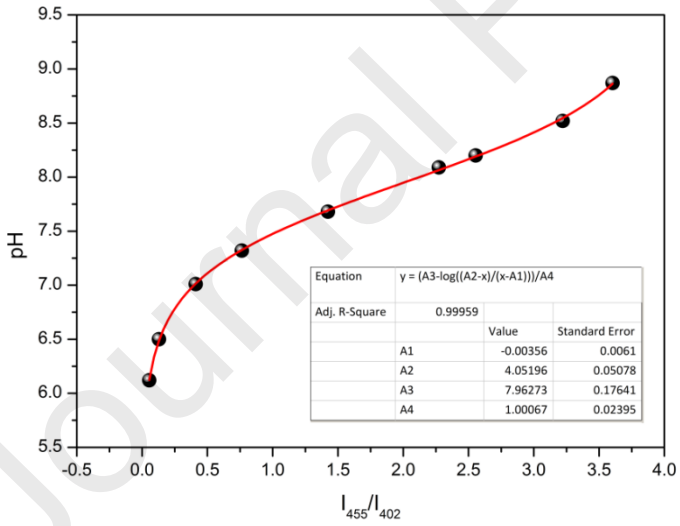

Figure S3. Representative pH calibration curve with HPTS concentration of 1.0 μg mL^{-1} (inset shows fitting results).

5. Limitation of PBO length obtained in DMF

βCD-based star PBOs bearing short PBO arms - βCD-$(PBO_m)_{14}$ (m = 6, 7, 8) were successfully synthesized in DMF, according to our previous work [1]. However, longer PBO arms (*e.g.,* m = 24) were not obtained under the same conditions as displayed in Table S2. The results indicate that the value of *m* is limited to 16 ± 3 (average ± StDev of $m_{theo.}$ of the 5 entries listed in Table S2) when homopolymerization was performed in DMF.

Table S2. Characteristics of βCD-$(PBO_m)_{14}$ synthesized in DMF.

Entry	$[BO]_0/[tBuP4]_0/[\beta CD]_0$[a]	*T* (°C)	*p*[b]	*f*[c]	$m_{theo.}$[d]	$Mn_{theo.}$[d] (kg mol^{-1})	Mn_{SEC}[e] (kg mol^{-1})	*Đ*[e]
1	339/2.8/1	25	0.76	0.99	18.2	20.4	15.6	1.03
2	588/2.8/1	25	0.38	0.97	15.5	17.6	12.4	1.03
3	604/2.8/1	30	0.30	0.96	12.4	16.4	8.8	1.04
4	613/2.8/1	30	0.49	0.85	18.2	20.4	17.7	1.04
5	589/7.0/1	30	0.44	0.79	14.6	16.8	5.8[e']	1.05[e']

[a]Various feeding ratios with constant initial monomer concentration as $[BO]_0$ = 3 M in DMF; [b]BO conversion (*p*) was determined by ^{1}H NMR; [c]The fraction of the star PBO (*f*) in product was estimated based on peak areas in SEC trace; [d]Theoretical value of *m* ($m_{theo.}$) was calculated based on monomer feeding ratio, monomer conversion and product purity. Theoretical molar mass ($Mn_{theo.}$) was determined based on $m_{theo.}$; [e,e']SEC characterizations were performed [e]in DMF at 60 °C or [e']in THF at 40 °C. The characterization results were determined with PMMA as the standard using a RI detector.

6. ^{1}H NMR and SEC characterizations of βCD-$(PBO_{24}$-$PGL_6)_{14}$

The reaction media obtained at the end of the two homopolymerizations and the copolymerization, for the synthesis of βCD-$(PBO_{24}$-$PGL_6)_{14}$, were characterized by ^{1}H NMR (Figure S4), providing the monomer conversions. The copolymerization product (after removing tBuP4) and the crude deprotection product were characterized by ^{1}H NMR (Figure S5), proving that the deprotection was effective. In parallel, these intermediate and final products were characterized by SEC (Figure 1 in main text). Table S3 gathers the characteristics of the star polymer in each product.

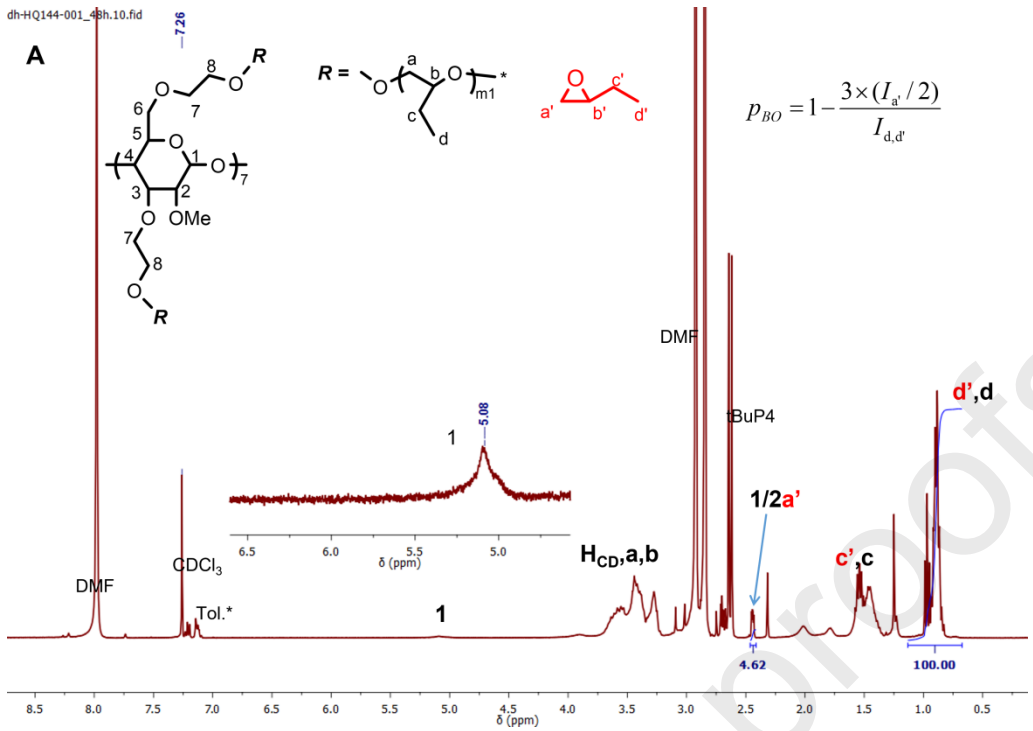

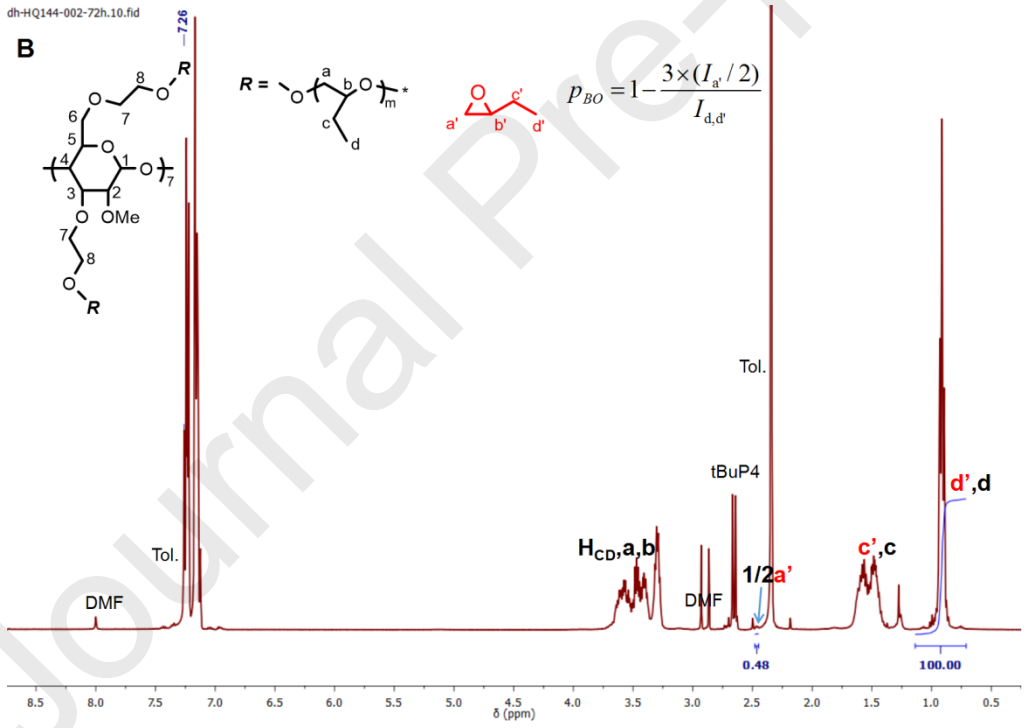

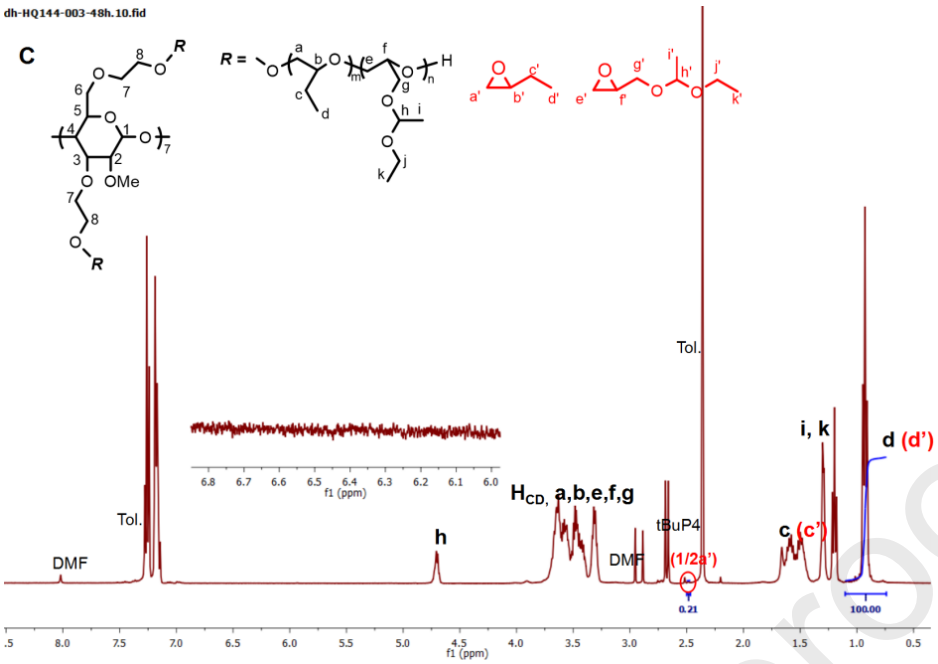

Figure S4. ^{1}H NMR spectra of the reaction media obtained in the synthetic procedure for βCD-(PBO$_{24}$-PGL$_6$)$_{14}$: at the end of (A) the first homopolymerization, (B) the second homopolymerization, and (C) the copolymerization. H$_{CD}$ stands for the protons in the βCD-based initiator, including protons 2, 3, 4, 5, 6 and 7. *Residual toluene in the initiator (spectrum A) originated from the drying pre-treatments. All spectra were recorded in $CDCl_3$ at 300 K.

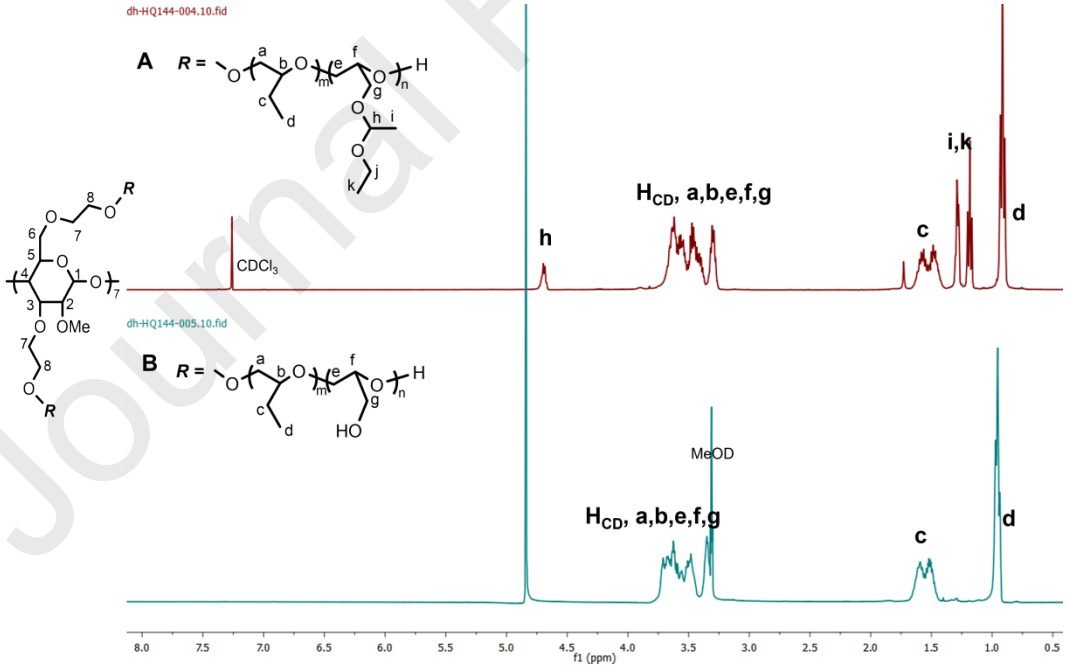

Figure S5. ^{1}H NMR spectra of (A) the copolymerization product (without tBuP4) and (B) the crude deprotection product obtained in the synthetic procedure for βCD-(PBO$_{24}$-PGL$_6$)$_{14}$. H$_{CD}$ stands for the protons in the βCD-based initiator, including protons 2, 3, 4, 5, 6 and 7. Spectrum A was recorded in $CDCl_3$-d1, B in MeOD-d4, both at 300 K.

Table S3. Characteristics of star polymers in the intermediate and final products in the synthetic route for βCD-(PBO$_{24}$-PGL$_6$)$_{14}$.

Polymer	p_{BO}[a]	p_{EEGE}[a]	f[b]	$m_{theo.}$[c]	$n_{theo.}$[c]	$Mn_{theo.}$[c] (kg mol^{-1})	Mn_{SEC}[d] (kg mol^{-1})	Đ[d]
βCD-(PBO$_{m1}$)$_{14}$	0.86	--	0.96	6.7	--	8.8	7.6	1.07
βCD-(PBO$_m$)$_{14}$	0.99	--	0.80	24.4	--	26.6	28.8	1.08
βCD-(PBO$_m$-PEEGE$_n$)$_{14}$	0.99	1	0.72	24.4	5.9	38.6	40.1	1.06
βCD-(PBO$_m$-PGL$_n$)$_{14}$ (*crude*)	--	--	0.84	24.4	5.9	32.7	35.5[d']	1.05[d']
βCD-(PBO$_m$-PGL$_n$)$_{14}$ (*purified*)	--	--	0.98	24.4	5.9	32.7	36.1[d']	1.05[d']

[a]Monomer conversions of BO (p_{BO}) and EEGE (p_{EEGE}) were calculated from ^{1}H NMR spectra; [b]The fraction of star polymer in each product (f) was estimated based on the peak areas in SEC trace; [c]Theoretical Xn values of PBO and PEEGE/PGL blocks per arm ($m_{theo.}$ and $n_{theo.}$, respectively) were estimated based on monomer feeding ratios, the values of p and f. Theoretical molar mass ($Mn_{theo.}$) was derived from the theoretical formula. [d,d']SEC characterizations were performed [d]in THF at 40 °C or [d']in DMF at 60 °C, and results were determined with PMMA as the standard and using a RI detector.

7. **The feasibility of the synthetic procedure of βCD-(PBO$_m$-PGL$_n$)$_{14}$**

The synthetic procedures as well as the characterization results of two other star copolymers, βCD-(PBO$_{13}$-PGL$_6$)$_{14}$ and βCD-(PBO$_6$-PGL$_{14}$)$_{14}$, respectively having medium and short PBO blocks were briefly introduced as below.

βCD-(PBO$_{13}$-PGL$_6$)$_{14}$ was prepared following the procedure illustrated in Scheme 1 in the main text, via a two-step homopolymerization, a sequential block copolymerization and a deprotection step. The intermediates and the crude product were characterized by ^{1}H NMR (Figure S6) and SEC (Figure S7A). The crude product was further purified via dialysis (RC membrane with MWCO 10k Da, against MeOH) and obtained after concentration. The quantity of the final product was confirmed by SEC (Figure S7B).

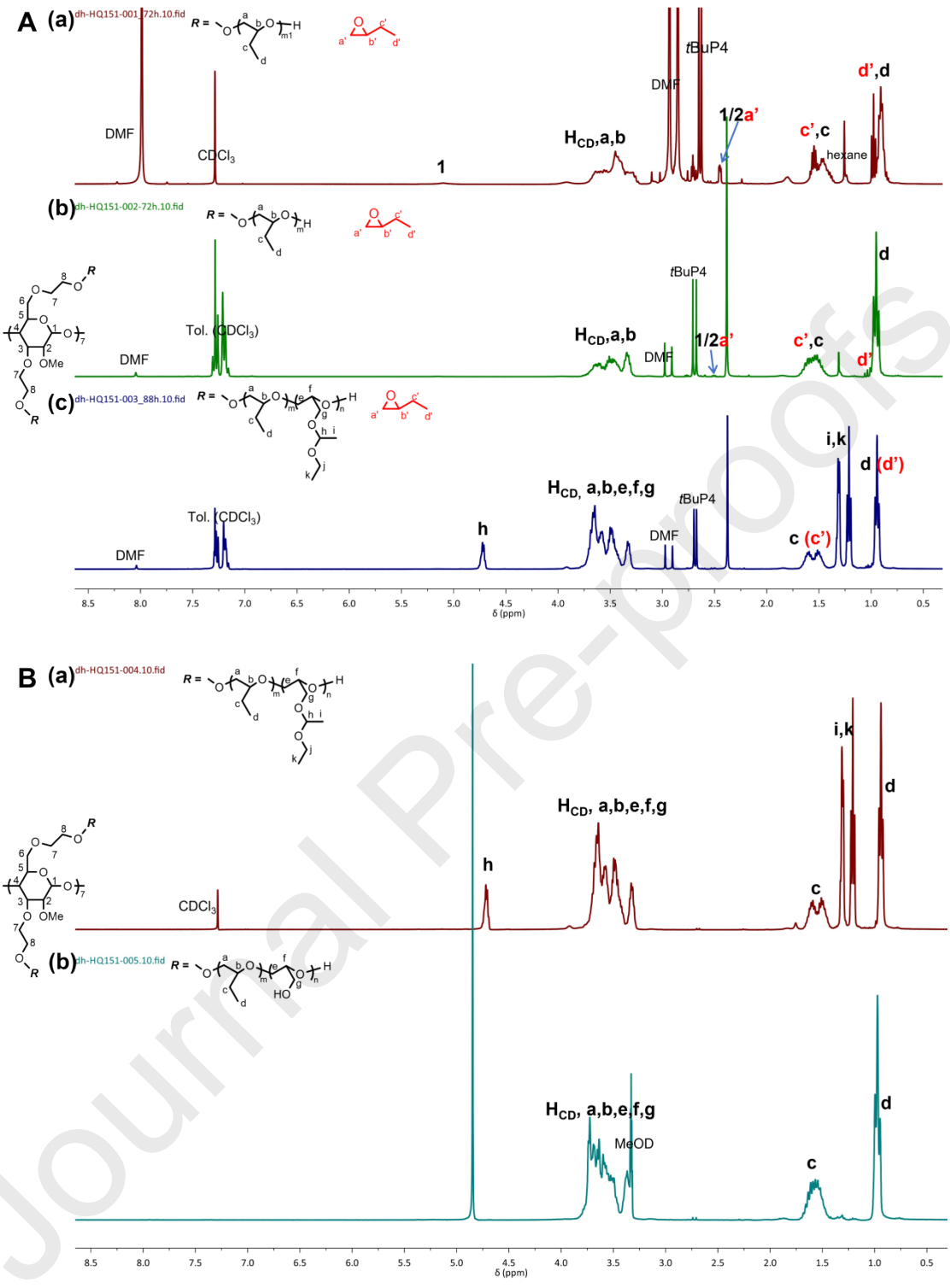

Figure S6. ^{1}H NMR spectra of (A) the reaction media obtained in the first homopolymerization (a), the second homopolymerization (b) and the sequential copolymerization (c), and (B) the polymers before (a) and after (b) deprotection in the synthetic process of βCD-$(PBO_{13}$-$PGL_6)_{14}$, recorded at 300 K, in $CDCl_3$ or MeOD according to the assignments. H_{CD} are the protons in βCD-based initiator, including protons 2,3,4,5,6,7.

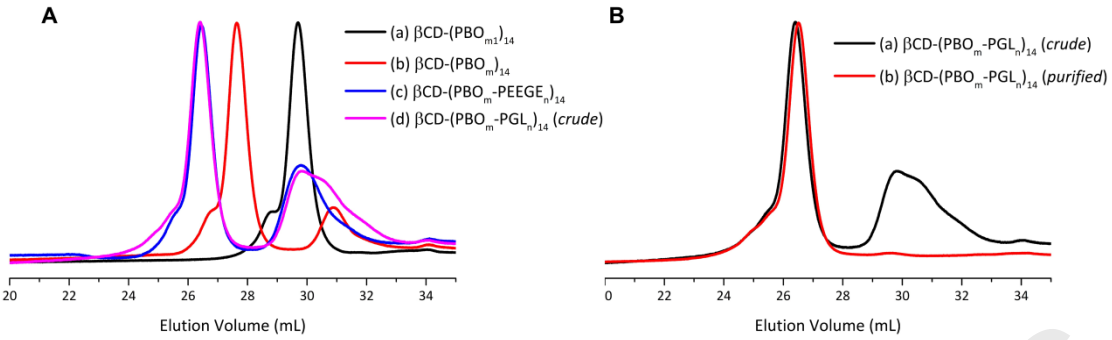

Figure S7. SEC traces of (A) the intermediates and crude deprotection product in the synthetic process of βCD-(PBO$_{13}$-PGL$_{6}$)$_{14}$, and (B) the deprotection products before and after purification. Characterizations were performed in DMF and recorded with a RI detector.

Derived from the characterization data, the characteristics of the star polymer in each intermediate and product were determined and listed in Table S4. The results indicate that the reactions were defined as the polydispersity indexes (*Đ*) were close to 1.1 and the molar masses characterized by SEC (Mn$_{SEC}$) were in consistent with the theoretical values (Mn$_{theo.}$).

Table S4. Characteristics of star polymers in the intermediate and final products in the synthetic route for βCD-(PBO$_{13}$-PGL$_{6}$)$_{14}$.

Polymer	p_{BO}[a]	p_{EEGE}[a]	f[b]	$m_{theo.}$[c]	$n_{theo.}$[c]	Mn$_{theo.}$[c] (kg mol^{-1})	Mn$_{SEC}$[d] (kg mol^{-1})	Đ[d]
βCD-(PBO$_{m1}$)$_{14}$	0.78	--	0.95	5.0	--	7.1	5.3	1.11
βCD-(PBO$_{m}$)$_{14}$	0.99	--	0.74	13.2	--	15.3	14.4	1.07
βCD-(PBO$_{m}$-PEEGE$_{n}$)$_{14}$	0.99	1	0.60	13.2	5.8	27.2	24.5	1.05
βCD-(PBO$_{m}$-PGL$_{n}$)$_{14}$ (*crude*)	--	--	0.59	13.2	5.8	21.4	25.5	1.08
βCD-(PBO$_{m}$-PGL$_{n}$)$_{14}$ (*purified*)	--	--	0.99	13.2	5.8	32.7	24.9	1.11

[a]Monomer conversions of BO (p_{BO}) and EEGE (p_{EEGE}) were calculated from ^{1}H NMR spectra; [b]The fraction of star polymer in each product (f) was estimated based on the peak areas in SEC trace; [c]Theoretical Xn values of PBO and PEEGE/PGL blocks per arm ($m_{theo.}$ and $n_{theo.}$, respectively) were estimated based on monomer feeding ratios, the values of p and f. Theoretical molar mass (Mn$_{theo.}$) was derived from the theoretical formula. [d]SEC characterizations were performed in DMF at 60 °C and results were determined with PMMA as the standard and using a RI detector.

βCD-$(PBO_6$-$PGL_{14})_{14}$ was prepared following the synthetic route including a one-step homopolymerization, a sequential block copolymerization and a deprotection step. The intermediates and the crude product were characterized by ^{1}H NMR (Figure S8) and SEC (Figure S9A) to track the reactions. At last, the crude product was purified via dialysis (RC membrane with MWCO 3.5k Da, against H_2O) and collected after freeze-dryness. The quantity of the purified product was confirmed by SEC (Figure S9B).

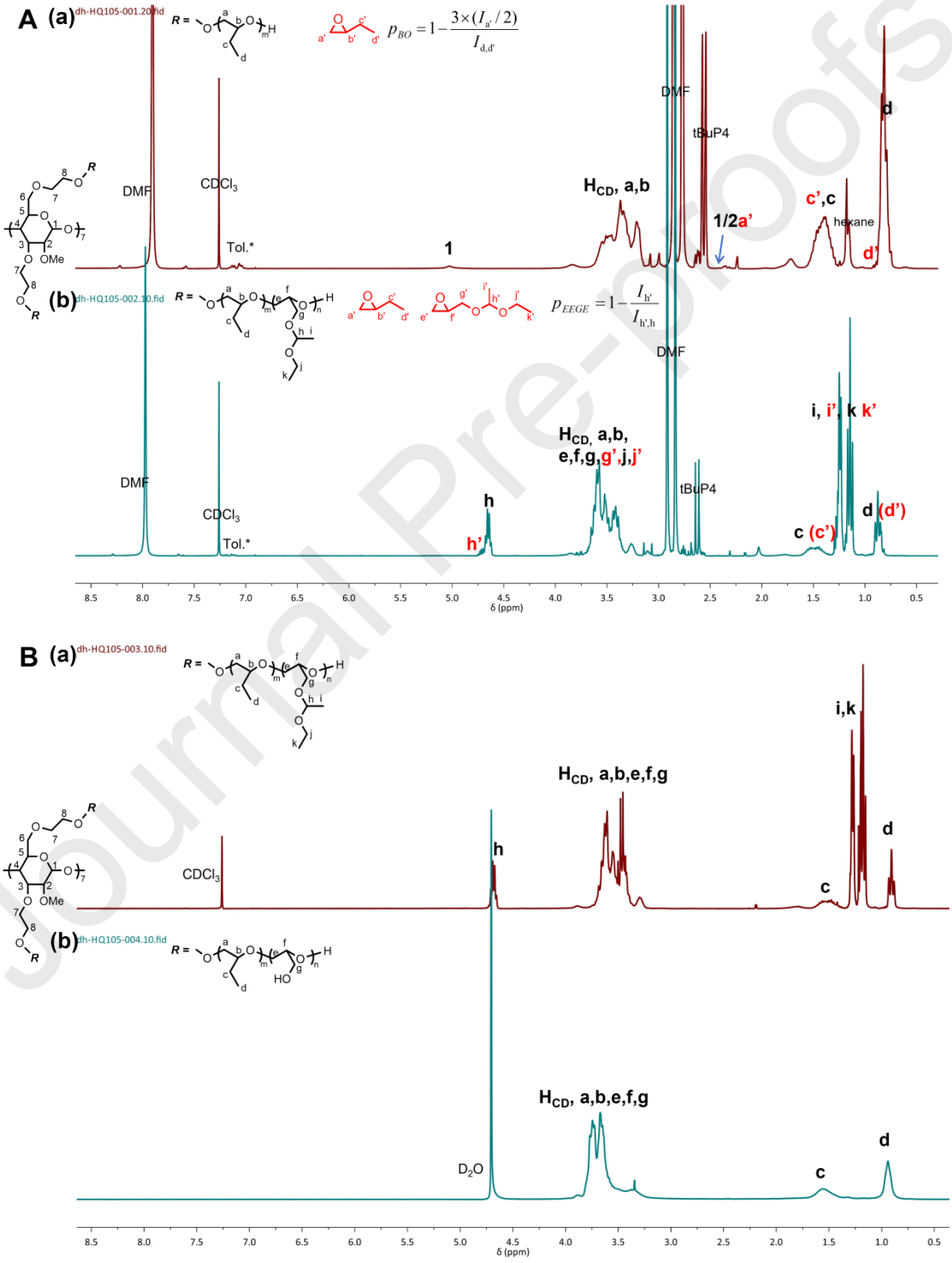

Figure S8. ^{1}H NMR spectra of (A) the homopolymerization (a) and copolymerization (b) media, and (B) the polymers before (a) and after (b) deprotection in the synthetic process of βCD-(PBO$_6$-PGL$_{14}$)$_{14}$, recorded at 300 K, in $CDCl_3$ or D_2O according to the assignments. H_{CD} are the protons in βCD-based initiator, including protons 2,3,4,5,6,7.

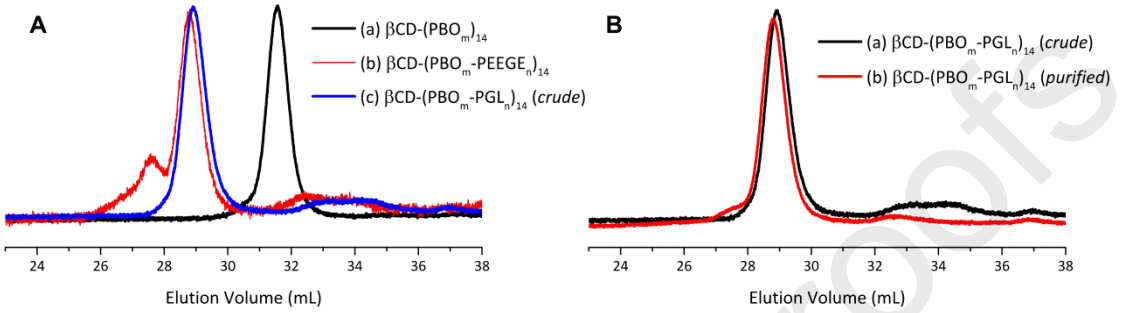

Figure S9. SEC traces of (A) the intermediates and crude deprotection product in the synthetic process of βCD-(PBO$_6$-PGL$_{14}$)$_{14}$, and (B) the deprotection products before and after purification. Characterizations were performed in DMF and recorded with a RI detector.

Based on the characterization data, the characteristics of the star polymer in each intermediate and product were determined and listed in Table S5. The results show that the polydispersity indexes (*Đ*) were small (close to 1.1) and the molar masses characterized by SEC (Mn$_{SEC}$) were in consistent with the theoretical values (Mn$_{theo.}$), indicating that the reactions were well defined.

Table S5. Characteristics of star polymers in the intermediate and final products in the synthetic route for βCD-(PBO$_6$-PGL$_{14}$)$_{14}$.

Polymer	p_{BO}[a]	p_{EEGE}[a]	f[b]	$m_{theo.}$[c]	$n_{theo.}$[c]	Mn$_{theo.}$[c] (kg mol^{-1})	Mn$_{SEC}$[d] (kg mol^{-1})	Đ[d]
βCD-(PBO$_m$)$_{14}$	0.98	--	0.99	6.4	--	8.5	8.3	1.03
βCD-(PBO$_m$-PEEGE$_n$)$_{14}$	0.98	1	0.89	6.4	13.5	36.1	27.8	1.08
βCD-(PBO$_m$-PGL$_n$)$_{14}$ (*crude*)	--	--	0.84	6.4	13.5	22.5	24.0	1.03
βCD-(PBO$_m$-PGL$_n$)$_{14}$ (*purified*)	--	--	0.94	6.4	13.5	22.5	25.9	1.06

[a]Monomer conversions of BO (p_{BO}) and EEGE (p_{EEGE}) were calculated from ^{1}H NMR spectra; [b]The fraction of star polymer in each product (f) was estimated based on the peak areas in SEC trace; [c]Theoretical Xn values of PBO and PEEGE/PGL blocks per arm ($m_{theo.}$ and $n_{theo.}$,

respectively) were estimated based on monomer feeding ratios, the values of *p* and *f*. Theoretical molar mass ($Mn_{theo.}$) was derived from the theoretical formula. [d]SEC characterizations were performed in DMF at 60 °C and results were determined with PMMA as the standard and using a RI detector.

Additionally, the well-defined ^{1}H NMR spectra and respective SEC traces of all βCD-cored star amphiphilic copolymers (Figure S10) demonstrate the proposed synthetic procedure is reproducible.

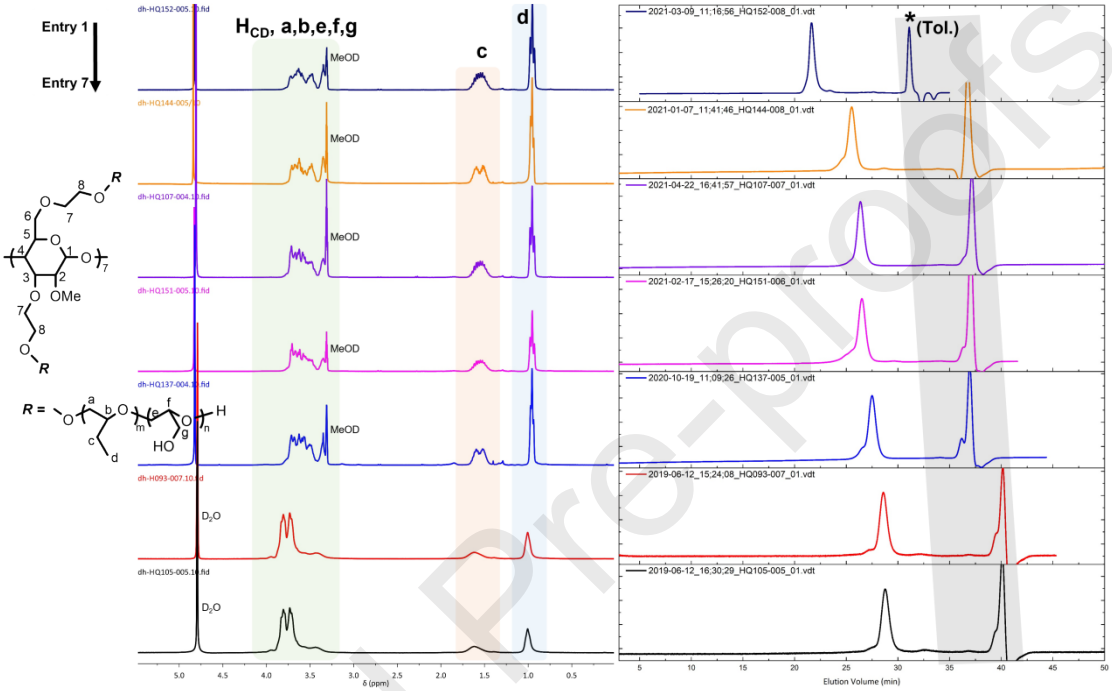

Figure S10. Stacked ^{1}H NMR spectra of βCD-cored star amphiphilic copolymers after deprotection (left panel) and SEC traces of respective purified products (right panel). From top to bottom are Entries 1 to 7, same as those in Table 1 of the main text. ^{1}H NMR spectra were recorded at 300 K in D_2O or MeOD according to assignments. H_{CD} are the protons in βCD-based initiator, including protons 2,3,4,5,6,7. SEC characterizations were performed in THF (Entry 1) or DMF (Entries 2-7) and recorded with a RI detector. *Tol. is the signal of the inner standard toluene as reference in SEC characterization.

8. Self-assembly behavior of βCD-(PBO-PGL)$_{14}$ compared to PGL-PBO-PGL

The self-assemblies were prepared via thin film rehydration followed with 5 extrusions through a 0.45 μm syringe filter. The first set of data was the observed data regarding to the appearance of the rehydrated suspensions before and after extrusions as well as the respective DLS data (Figure S11).

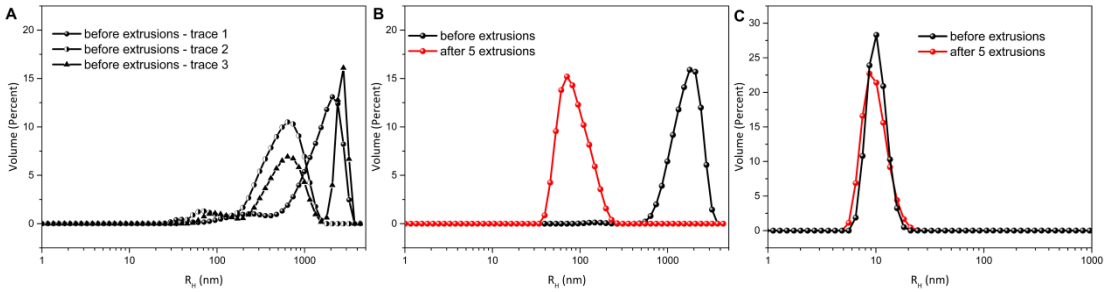

Figure S11. The particle size distribution curves of the rehydrated suspensions of (A) βCD-$(PBO_{24}$-$PGL_6)_{14}$ before extrusions, and the curves of (B) βCD-$(PBO_{13}$-$PGL_6)_{14}$ and (C) βCD-$(PBO_6$-$PGL_{14})_{14}$ before and after extrusions. The ill-aggregates formed by βCD-$(PBO_{24}$-$PGL_6)_{14}$ were removed after extrusions.

The self-assembly behavior of star copolymers (βCD-$(PBO$-$PGL)_{14}$) in aqueous solution (1 mg mL^{-1} in H_2O) was studied using DLS and SAXS techniques. The results, including DLS data (Figure 2A and Figure S12A) and SAXS data (Figure 2B and Figure S12B) indicate that the self-assembled morphology was highly decided by the weight fraction of PGL block (w_{PGL}).

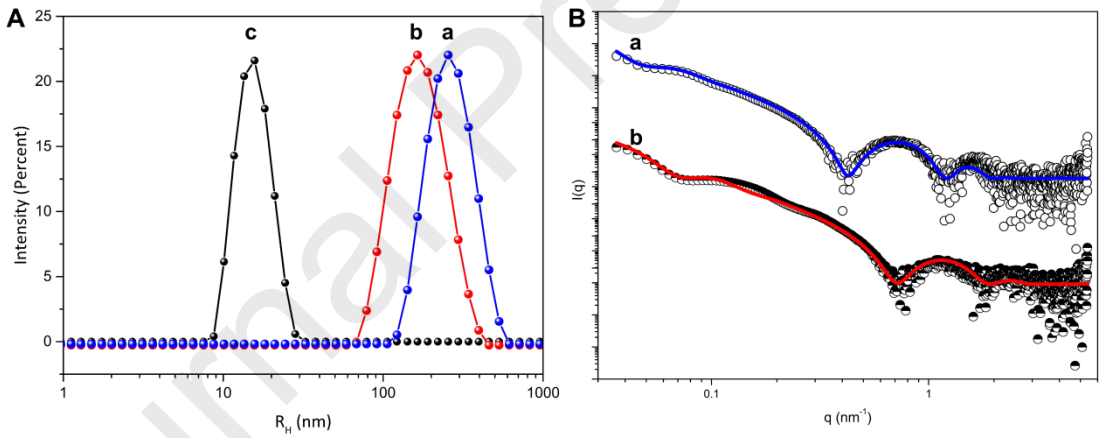

Figure S12. (A) The particle size distribution curves of (a) βCD-$(PBO_{22}$-$PGL_7)_{14}$, (b) βCD-$(PBO_7$-$PGL_5)_{14}$ and (c) βCD-$(PBO_8$-$PGL_{12})_{14}$, and (B) SAXS profiles (dots) of the self-assemblies of (a) βCD-$(PBO_{22}$-$PGL_7)_{14}$ and (b) βCD-$(PBO_7$-$PGL_5)_{14}$ as well as respective fitting curves (solid lines) obtained by fitting using a vesicle form factor.

Based on the available data, the morphology evolution scheme was profiled (Scheme S1, bottom), which closely resembles that of linear analogues (Scheme S1, top; based on the data listed in Table S1).

Scheme S1. Morphology evolution with the weight fraction of PGL blocks (w_{PGL}) of βCD-$(PBO$-$PGL)_{14}$ (bottom) and PGL-PBO-PGL (top).

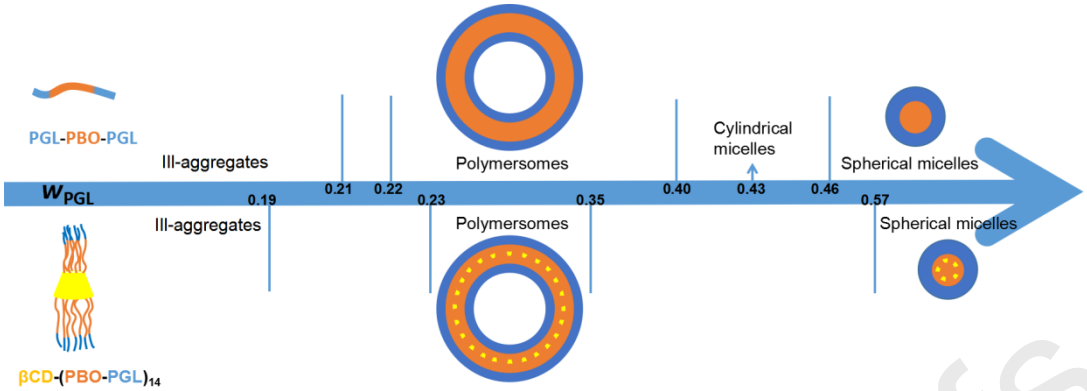

9. Thickness attributed to PBO segments (t_{PBO}) in polymersome membranes

The thickness attributed to PBO segments (t_{PBO}) in the polymersomes made from βCD-(PBO-PGL)$_{14}$ were derived from small-angle X-ray scattering (SAXS) characterization, being $t_{PBO} = t_t - H_{CD}$ with t_t the thickness of hydrophobic layer derived from SAXS and H_{CD} the thickness of βCD (0.78 nm [6]) (Scheme S2 and Table S6). As a comparison, t_{PBO} values of PGL-PBO-PGL polymersomes were also determined, being $t_{PBO} = t_t$ (Scheme S2 and Table S6). For clarity, Scheme S2 illustrates the bilayered structures concerning the polymersomes made from linear and star copolymers.

Scheme S2. Graphical descriptions of the polymersomes made from PGL-PBO-PGL (left) and βCD-(PBO-PGL)$_{14}$ (middle) as well as the βCD-(PBO-PGL)$_{14}$ structure (right). Blue and yellow layers respectively describe PGL and PBO segments and the golden blocks indicate βCD.

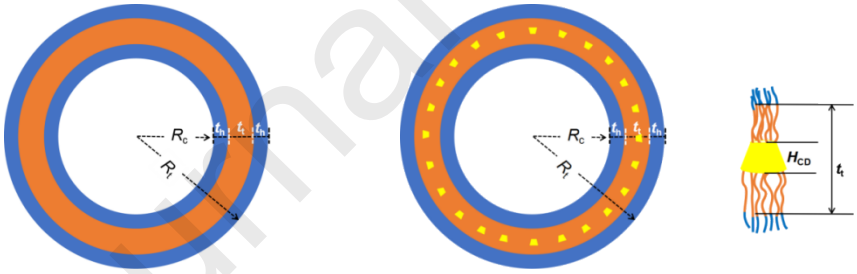

Table S6. Structural parameters of polymersomes derived from SAXS analyses, according to the *X*n of PBO blocks.

Polymersomes	t_t^a **(nm)**	t_{PBO}^b **(nm)**	t_h^a **(nm)**	R_c^a **(nm)**	R_t^a **(nm)**
βCD-(PBO-PGL)$_{14}$					
βCD-(PBO$_7$-PGL$_5$)$_{14}$	3.2	2.42	1.7	36.2	42.8
βCD-(PBO$_{13}$-PGL$_6$)$_{14}$	4.4	3.62	2.3	49.9	59.0
βCD-(PBO$_{22}$-PGL$_7$)$_{14}$	5.6	4.82	2.2	52.5	62.6
PGL-PBO-PGL					

PGL_6-PBO_{20}-PGL_6	2.9	2.9	1.8	52.5	59.0
PGL_6-PBO_{40}-PGL_6	4.3	4.3	2.0	44.4	52.7
PGL_{20}-PBO_{59}-PGL_{20}	5.7	5.7	2.7	54.8	66.0
PGL_{18}-PBO_{62}-PGL_{18}	6.1	6.1	3.6	61.0	74.3
PGL_{25}-PBO_{80}-PGL_{25}	7.3	7.3	2.8	42.8	55.6
PGL_{12}-PBO_{84}-PGL_{12}	6.7	6.7	2.9	56.1	68.6
PGL_{21}-PBO_{84}-PGL_{21}	6.8	6.8	3.6	51.9	65.9

[a] t_t, t_h, R_c and R_t are the structural parameters illustrated in Scheme S2; [b] $t_{PBO} = t_t - H_{CD}$ (for βCD-$(PBO\text{-}PGL)_{14}$ polymersomes) or t_t (for PGL-PBO-PGL polymersomes).

10. Permeability of polymersomes to H^+

In the investigation, we found the pH_f decaying plots of HPTS solutions of varied concentrations were different, although they were produced following the same protocol. To minimize the potential influence of HPTS concentration on the results, for each HPTS-pos, the respective control experiment was conducted, with the HPTS solution having the same HPTS concentration as that in the bulk HPTS-pos suspension.

The HPTS concentration of bulk HPTS-pos solution was determined based on a calibration curve. Specially, five working HPTS solutions of varied concentrations, in a mixture of solvents of 0.3 mL PBS, 0.7 mL DI H_2O and 2.0 mL MeOH, were prepared. The excitation spectrum of each working solution was recorded 5 times on a Cary Eclipse fluorophotometer at room temperature with emission wavelength being 509 nm and ex-slit and em-slit both 5 nm. The average excitation intensity at 402 nm (I_{402}) was plotted against concentration producing the calibration curve. Then, 0.3 mL HPTS-pos suspension solution was dissolved with a mixture of 0.7 mL DI H_2O and 2.0 mL MeOH, and the excitation spectrum of the resulted solution was recorded 5 times under the same conditions as those applied for the construction of calibration curve. At last, by substituting I_{402} into the concentration calibration curve, the HPTS solution of the bulk HPTS-pos suspension solution was obtained, as listed in Table S7.

Table S7. HPTS concentrations of bulk HPTS-pos suspensions and HPTS solutions in respective control experiments, according to the hydrophobic thickness of the polymersomes (t_t)[a].

Entry	**Polymersome**	t_t[a] **(nm)**	**HPTS concentration (μg mL^{-1})**	
			HPTS-pos suspension	**HPTS solution**
a	PGL_{25}-PBO_{80}-PGL_{25}	7.3	0.82	0.82

b	PGL_{21}-PBO_{84}-PGL_{21}	6.8	1.05	1.05
c	PGL_{18}-PBO_{62}-PGL_{18}	6.1	2.34	2.34
d	PGL_{6}-PBO_{40}-PGL_{6}	4.3	0.82	0.82
e	βCD-$(PBO_{13}$-$PGL_{6})_{14}$	4.4	1.31	1.31

[a]The thickness of the hydrophobic layer of polymersomes (t_t) was determined by SAXS.

References

1. Faye I, Huin C, Illy N, et al. β-Cyclodextrin-Based Star Amphiphilic Copolymers: Synthesis, Characterization, and Evaluation as Artificial Channels. Macromolecular Chemistry and Physics, 2019, 220(2): 1800308.

2. Taton D, Borgne AL, Sepulchre M, et al. Synthesis of chiral and racemic functional polymers from glycidol and thioglycidol. Macromolecular Chemistry and Physics, 1994, 195: 139-148

3. Du H, de Oliveira F A, Albuquerque L J C, et al. Polyglycidol-Stabilized Nanoparticles as a Promising Alternative to Nanoparticle PEGylation: Polymer Synthesis and Protein Fouling Considerations. Langmuir, 2020, 36(5): 1266-1278.

4. Paxton W F, Price D, Richardson N J. Hydroxide ion flux and pH-gradient driven ester hydrolysis in polymer vesicle reactors. Soft Matter, 2013, 9(47): 11295-11302.

5. Wu J, Eisenberg A. Proton diffusion across membranes of vesicles of poly(styrene-b-acrylic acid) diblock copolymers. Journal of the American Chemical Society, 2006, 128(9): 2880-2884.

6. Van De Manakker F, Vermonden T, Van Nostrum C F, et al. Cyclodextrin-based polymeric materials: synthesis, properties, and pharmaceutical/biomedical applications. Biomacromolecules, 2009, 10(12): 3157-3175.

Philippe Guégan

Professeur Sorbonne Université

Institut Parisien de Chimie Moléculaire UMR 8232

Chimie des Polymères

July 19th, 2022

Dear Editor,

Declaration of interests

The authors declare that they have no known competing financial interests or personal relationships that could have appeared to influence the work reported in the manuscript entitled "**Engineering of Ion Permeable Planar Membranes and Polymersomes based on β-Cyclodextrin-Cored Star Copolymers**" by Du *et al*.

Best regards,

P. Guégan

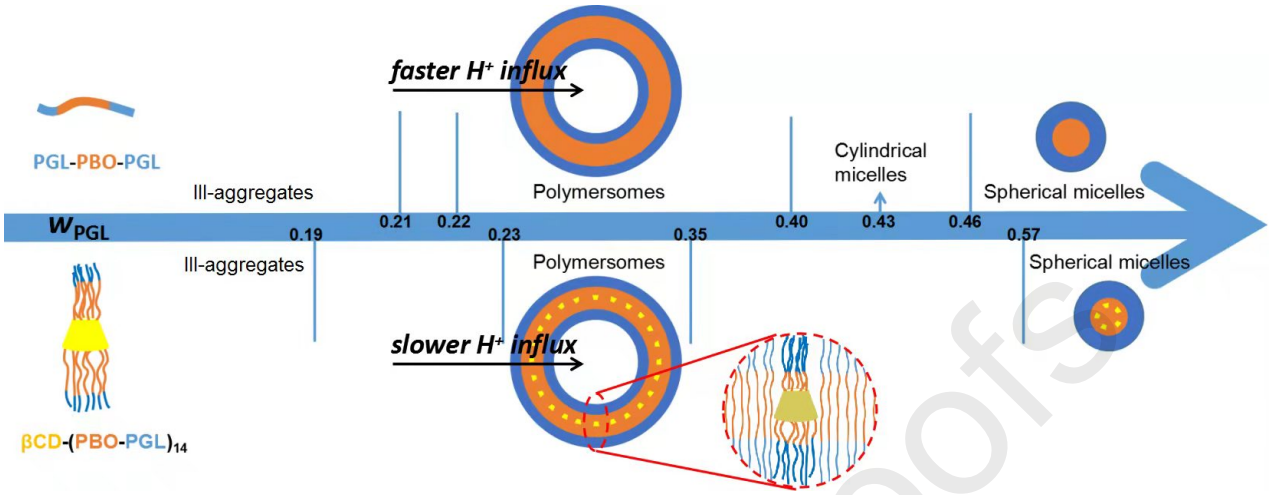

Haiqin Du : Data curation, Investigation, writing orginal draft, Sandra Kalem : data curation ; Cécile Huin : Data curation, Formal analysis, validation ; Nicolas Illy : supervision ; Guillaume Tresset : Data curation, formal analysis, validation ; Fernando Giacomelli : conceptualization, funding acquisition, investigation, methodology ; Philippe Guégan : conceptualization, funding acquisition, investigation, project administration.